Chapter 13 in the book:
P.A. Kralchevsky and K. Nagayama, "Particles at Fluid Interfaces and Membranes," Elsevier, Amsterdam, 2001; pp. 517–590

CHAPTER 13

TWO-DIMENSIONAL CRYSTALLIZATION OF PARTICULATES AND PROTEINS

First we give an overview of the methods for producing ordered 2D arrays from colloid particles and proteins in relation to their physical mechanisms and driving forces. From this viewpoint the following methods can be distinguished: evaporation of liquid suspension films; ordering owing to Kirkwood-Alder transition at high particle concentrations; self-assembly of colloidal particles at a single fluid interface; ordering of particles forced by the action of applied external electric, magnetic or optical fields; structuring in insoluble particle monolayers in a Langmuir trough, and ordering due to the binding of particles at structured adsorption sites.

The major part of this chapter is devoted to the method for obtaining particle and protein 2D arrays in *evaporating liquid suspension films*; this method is closer to the subject of the present book and to the research fields of the authors. The respective mechanism of 2D crystallization is based on the fact that the decrease of the film thickness (because of evaporation) forces the particles to enter and/or deform the liquid interface, which automatically "switches on" the strong attraction due to the capillary immersion force. The latter collects the particles into ordered aggregates, which further grow owing to an evaporation-driven influx of new particles. Such evaporating films can be formed by spreading of protein solution in a mercury trough, which has been applied to crystallize dozens of proteins. Special attention is paid to the occurrence and advantages of 2D array formation over a liquid substrate: fluorinated oil and mercury. The particle size separation during 2D crystallization and the methods for obtaining large 2D-crystalline coatings on solid substrates are described. We consider also the formation of 2D arrays in free foam films and their observation by electron cryomicroscopy, which ensures an excellent structure preservation of delicate vesicles or molecular complexes. Finally we review the various applications of *particulate* 2D arrays in optics, optoelectronics, nano-lithography, microcontact printing, in fabrication of nanostructured surfaces for catalytic films and solar cells, as well as the usage of *protein* 2D crystals for immunosensors and extremely isoporous ultrafiltration membranes, for creation of bioelectronic and biophotonic devices, etc.

13.1. METHODS FOR OBTAINING 2D ARRAYS FROM MICROSCOPIC PARTICLES

In 1959 R. Feynman attracted the attention of the scientists at a huge unexplored field for a future development of research and technology: that is to manipulate matter on very small scale and to create nanodevices and nanotechnologies, see e.g. Ref. [1]. Since that time much has been done in this field, but an enormous amount still remains to be done. The achievements and the perspectives are summarized in several recent books on nanotechnology [2], microfabrication [3], biomolecular electronics [4-6]. A necessary step of a microfabrication is to order macromolecules or particles into structures and to interconnect them [7].

Some proteins can form three-dimensional (3D) and two-dimensional (2D) crystals due to specific molecular interactions and molecular recognition [8-12]. In other cases macromolecules or colloidal particles can form ordered 3D and 2D structures, called colloid crystals, under the action of nonspecific physical interactions [13,14]. The term "ordered array" is also used as a synonym of "colloidal crystal" [15]. Our attention in the present chapter will be focused on the methods for obtaining ordered 2D arrays from protein molecules and colloidal particles. In Section 13.8 we review their practical applications.

13.1.1. FORMATION OF PARTICLE 2D ARRAYS IN EVAPORATING LIQUID FILMS

In his work on determining the Avogadro number Perrin [16] measured the size of sub-μm particles by forming a 2D array of the particles on a solid substrate. He used an aqueous suspension containing monodisperse spheres of gomme-gutte. Some amount of this suspension was deposited on a glass substrate. After the water evaporated, Perrin observed and photographed particle 2D arrays.

Much work in the field of colloidal crystals were carried out with monodisperse spherical latex particles. They were first obtained by emulsion polymerization and examined with the help of electron microscopy by Backus and Williams [17]. Alfrey et al. [18] studied the optical properties of colloid crystals obtained by drying of aqueous latex suspensions; 14 different monodisperse samples, having particle diameters from 165 to 986 nm, were used. The diffraction of light from some of the crystalline samples was shown to be that for a two-

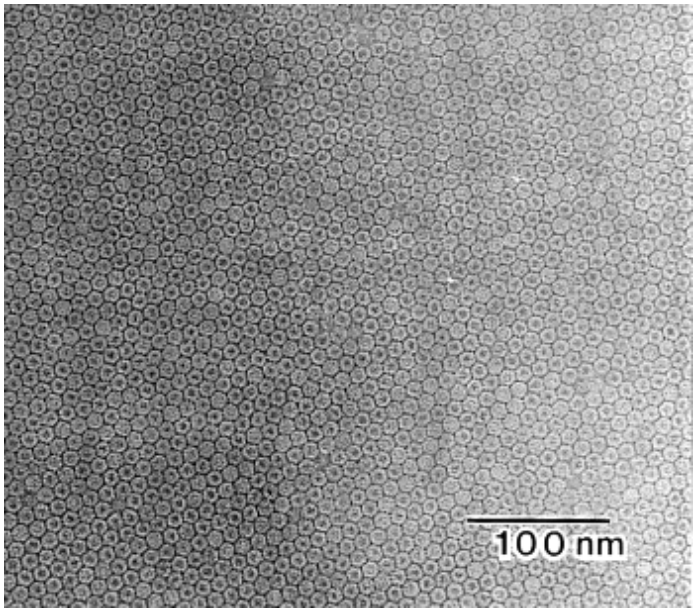

Fig. 13.1. Electron micrograph of a two-dimensional crystal of the protein ferritin, obtained by Yoshimura et al. [32] by means of the mercury trough method.

dimensional grating. It was proposed to use the latex crystals as diffraction gratings [18] and as standards for calibration of electronic microscopes [17,19]. Since then many authors have obtained ordered 2D arrays of latex spheres by evaporation from suspension layers, however it is not easy to obtain large mono-crystalline domains without a special control of the conditions, see Ref. [20] for details.

In 1945 Price et al. [21] evaporated an aqueous suspension of a purified plant virus (southern bean mosaic virus, bushy stunt virus and tobacco necrosis virus) deposited on a collodion-covered screen used for electron microscopy. The electron micrographs sowed that each of these viruses had formed 2D (and sometimes 3D) crystals over the substrate. In a similar way crystals from other plant viruses were obtained [22,23]. In 1974 Horne and Pasquali Ronchetti [24] formulated the *negative staining-carbon film method* for preparing 2D arrays of viruses and proteins. As a necessary step this method involves spreading and drying of suspension on a solid substrate. In this way, 2D crystals of various viruses [25,26] and proteins [27-30] have been obtained. Yoshimura et al. [31,32] spread protein suspension on the surface of mercury in a special mercury trough. After the evaporation of water large ordered protein 2D arrays were obtained (Fig. 13.1). This method was applied to crystallize a dozen of proteins, see Section 13.2.

The mechanism of 2D crystallization in evaporating films from suspensions on solid substrate has been investigated in details by Denkov et al. [33,34] in experiments with latex spheres in a specially designed experimental cell. The direct observations of the dynamics of array formation reveals that the nucleation and growth of the 2D colloid crystals is governed by an interplay of the lateral immersion force (Chapter 7) and an evaporation-driven convective flow, see Section 13.3.1 for details.

Similar experimental setup has been used by Dushkin et al. [35,36] to study the kinetics of 2D-array growth and the color phenomena observed with ordered multilayers from sub-μm latex spheres on solid substrate (Section 13.3.2). Subsequent experiments confirmed that the mechanism of ordering, established by Denkov et al. [33,34] for wetting films on solid substrate, is operative also in the case of 2D crystallization on liquid substrates: fluorinated oil [37] and mercury [38], see Section 13.4 below. Yamaki et al. [39] observed experimentally and simulated by computer a phenomenon of size separation of sub-μm particles (latex spheres, viruses, proteins) during 2D crystallization; this is an additional evidence for the action of the lateral immersion force (see Section 13.5).

Large 2D-crystalline coatings from latex particles have been obtained by Dimitrov and Nagayama [40,41] by pulling up a plate out of a suspension with a controlled speed. An wetting film is deposited after the receding meniscus, in which the colloidal particles are ordered under the combined action of the capillary forces and the evaporation-driven convective flux. The deposition of a wetting film containing colloidal particles, and subsequent formation of large uniform 2D arrays, is possible also by deposition with a plate (playing the role of a brush) [42] or by continuous supply of the suspension with the help of an extruder [43], see Section 13.6.

Ordered 2D arrays can be obtained not only in wetting films, but also in free foam films [44-47]. To observe the arrays from sub-μm particles in such a foam film, the latter can be quickly frozen and examined by electron microscopy [44-46]; in this way arrays from delicate “soft” particles, like lipid-protein vesicles or surfactant micelles, could be observed (Section 13.7).

It should be noted that large and well ordered particle monolayers can be formed under controlled conditions, which give the possibility to adjust the rate of receding of the liquid

meniscus equal to the rate of growth of the ordered array due to the supply of particles by the evaporation-driven convective flux [33-45]. In the absence of such a control it is possible to find only small ordered clusters or separate domains [48-50].

If simply a sessile drop (having the shape shown in Fig. 2.13) of the suspension is evaporated one observes only a narrow monolayered zone in the feet of a multilayered hill of particles, which has a ring-shape; in other words, the particles contained in the droplet are deposited in a vicinity of the *receding* contact line of the drying drop, see Section 13.3.1. The formation of such ring-shaped deposits by drying sessile drops has been examined by Deegan et al. [51]. In a similar way Maenosono et al. [52] obtained and investigated rings of semiconductor nanoparticles. Ring-shaped structures from particles can be created also by an *expanding* contact line: if a thinning suspension film is unstable and breaks, the contact line of the growing hole collects the particles into an annular ring-like array [53].

The simplest way to obtain a uniform monolayered domain, instead of multilayered ring, is to place a suspension drop on a substrate and then to smear it with a glass rod, before the drying [54]. A more elaborated way is to apply the *spin-coating* technique (spreading of a droplet over a rotating substrate) [50,55-57], which is currently used in industry to make polymeric films. Varying the particle concentration and spin speed, one could reproducibly fabricate monolayers and bilayers of hexagonal packing [58].

Another relatively simple method was introduced by Micheletto [59]: a drop of the colloid suspension is placed on a glass plate, which is then tilted at an appropriate angle. Thus the array formation starts at the upper edge of the drop and proceeds downwards. This method was applied by Burmeister et al. [60], who afterwards stabilized the monolayer by vacuum deposition of a metal or by thermal annealing. Further, the substrate was slowly dipped into water and the stabilized ordered particle monolayer gradually floated off as a whole onto the water surface. The floating array was finally transferred onto the desired surface [60].

Ordered particle monolayers of good quality can be produced if a drop of suspension is spread on a solid substrate encircled with a Teflon ring, as demonstrated by Denkov et al. [33]. Thus a slightly concave meniscus is formed, which leads to initiation of the ordering in the middle of the encircled area (see Section 13.3.1). In this way Du et al. [61] obtained ordered

monolayers from monodisperse copolymer latex spheres of diameter less than 100 nm. The authors varied the concentrations of electrolyte and surfactant (emulsifier) in order to improve the quality of the ordered arrays. Likewise, with the help of a Teflon ring Sasaki and Hane [62] assembled polystyrene latex particles (diameter 64, 137 and 330 nm) and gold particles (diameter 39 nm) into regular 2D arrays on a glass substrate. To improve the quality of the array the authors applied an ultrasonic radiation technique. The ultrasonic radiation (frequency 2.4 MHz) increases the temperature of water (from 18 to 30 °C) and controlling its power one can adjust the evaporation. In addition, the treatment with ultrasonic waves manipulates the array in such a way that densely packed lattice is formed, whereas the appearance of voids and random assemblies is reduced [62].

As already noted, the method for obtaining 2D ordered particle arrays in evaporating liquid films can be applied also to form 2D ordered arrays of protein macromolecules. For example, Haggerty et al. [63] spread 10 μl droplets of aqueous protein solutions (lysozyme or chymotrypsinogen A) on freshly cleaved pyrolytic graphite. The samples were dried at room temperature for about 30 min and then examined by electron microscopy. Regular two-dimensional arrays of protein molecules were seen [63]. Likewise, by evaporation of the solvent from suspension films, ordered 2D arrays of inorganic particles on graphite [64] and amidine latex on mica [65] have been assembled.

As mentioned above, the ordering of particles in evaporating films is promoted by the attractive capillary immersion forces and the directional influx of particles driven by the evaporation (see Section 13.3 for details). On the other hand, it should be noted that in some cases particle ordering in liquid films is observed even when the latter two factors are missing. Such cases are considered in the next Section 13.1.2.

13.1.2. Particle ordering due to a Kirkwood-Alder type phase transition

Three-dimensional and two-dimensional colloid crystals can be formed also in the absence of attractive forces between the particles, if only the particle volume fraction is high enough. First, this type of disorder-order phase transition has been theoretically predicted by Kirkwood et al. [66,67] and then confirmed by computer simulations by Alder and Wainwright [67,68]

for a system of hard disks and hard spheres. It is usually termed the Kirkwood-Alder phase transition. The freezing point and the melting point for 3D systems were respectively estimated to be at particle volume fractions 0.50 and 0.55 [70]. Subsequent computer experiments showed that the same kind of first-order phase transition is observed for "soft" spheres, repelling each other electrostatically (the inverse power potentials) [71].

The essential feature of the Kirkwood-Alder phase transition is that it occurs between particles interacting only via *repulsive* forces. Such a phase transition was observed by Hachisu et al. [13] in suspensions of monodisperse latex particles and attributed by Wadati and Toda [72] to a Kirkwood-Alder transition. The existence of this phase transition in the bulk of latex suspensions was confirmed by many succeeding experimental works [73-77].

When the particles are situated in a vicinity of a planar interface (wall), or in a liquid film sandwiched between two interfaces, the particle structuring is facilitated by the ordering effect of the wall [78-82]. This is the same effect, which leads to the appearance of stratification with foam films [83] and gives rise to the oscillatory surface forces detected by the surface force apparatus [84], see Section 5.2.7.

Pieranski et al. [85] investigated experimentally a layer of deionized latex suspension confined between two glass surfaces: a flat plate and a sphere. Ordering of the latex particles has been observed. In subsequent studies Pieranski et al. [86,87] examined a deionized latex suspension (particle diameter 1.1 μm) contained in the wedge-shaped gap between two planar glass plates. It was observed that with the increase of the gap thickness a consequence of ordered monolayer, bilayer, trilayer, etc. had been formed in which the particles had alternatively changing triangular and square packing as follows: 1Δ–2❑–2Δ–3❑–3Δ–⋯ (the cipher denotes the number of layers and the symbol indicates the type of packing).

Similar experiments were carried out later by Van Winkle and Murray [88] with smaller polystyrene latex spheres (diameter 305 nm). The suspension was subjected to deionization, so 3D arrays were present also in the bulk. For gap thickness $h \approx 1$ μm the authors detected formation of a hexagonally ordered particle monolayer. As h increased, the evolution from two- to three-dimensional crystals was observed as a series of structural transitions, which

resembled that established by Pieranski et al. [86,87]. A melting transition was also detected [89].

Since the Kirkwood-Alder phase transition occurs in the absence of attraction between the particles, it cannot be classified as a self-assembly process. The volume restriction effect forces the particles to form ordered 3D and 2D arrays in this case. Such conditions of volume restriction are created when a colloidal dispersion, driven by the capillary action, fills the micro-channels of specially designed micromolds [90]. This micromolding method was used to prepare patterned arrays of polystyrene microspheres and other microscopic structures [90,91].

13.1.3. SELF-ASSEMBLY OF PARTICLES FLOATING ON A LIQUID INTERFACE

As described in details in Chapter 8, the weight of floating colloidal particles, of diameter bigger than 5-10 μm, is large enough to deform the fluid interface and to bring about interparticle attraction and agglomeration due to the lateral flotation force. Bowden et al. [92] prepared regular arrays of topologically complex, millimeter-scale objects, floating on the interface between perfluorodecalin and water. Ordered patterns of different topology were obtained by making hydrophilic or hydrophobic specified edges of the particles.

For particles smaller than 5 μm the lateral flotation force is usually negligible; an estimate can be made with the help of Eq. (8.2). Then if self-assembly of such small floating particles is observed, it can be attributed either to the van der Waals attractive surface force [93], or to the Lucassen's [94] capillary force between particles with undulated contact line (Chapter 12) for details. The energy W_{vw} of van der Waals attraction between two identical spherical particles of radius R, can be estimated by means of the Derjaguin approximation (Section 5.1.4):

$$W_{vw} = -\frac{A_H R}{12h} \tag{13.1}$$

where A_H is the Hamaker constant, and h is the surface-to-surface distance between the particles. Taking typical values, $A_H = 5 \times 10^{-20}$ J and $R = 1$ μm, one estimates that W_{vw} becomes equal to the energy of the thermal motion, kT, at distance $h = 1.02$ μm. In other words, the van der Waals attraction can be significant for such comparatively large Brownian

particles, and its range can be of the order of the particle radius. Note that the value $A_H = 5 \times 10^{-20}$ J is applicable to latex particles interacting across air. If the particles interact across water, A_H is about 10 times smaller [84], and then the effect of the van der Waals forces is significant only at close contact. Hence, the latter effect is expected to be more pronounced for floating hydrophobic particles, whose close contact is realized across the air phase.

In many cases the surface of the colloidal particles is not smooth, but it has some wave-like folds and/or edges. For example, some samples of latex "spheres" have corrugated surfaces. When attached to a fluid interface such particles exhibit undulated contact lines, and the Lucassen's capillary forces are expected to be operative. The latter are physically significant at distances equal to, or smaller than, the wavelength of the undulations, see Chapter 12.

Pieranski [14] examined by optical microscope a layer of latex suspension deposited on a glass substrate. The diameter of the polystyrene spheres was 245 nm. The thickness of the layer was decreased from a few microns to zero. For layer thickness about 300 nm only one layer of particles remained. When the thickness of the water layer was decreased rapidly, the particles were transferred from the bulk onto the water-air surface and were observed to form there ordered or disordered arrays, respectively, for higher and lower particle concentration. The observed uniform distribution of the particles indicated the existence of electrostatic repulsion. In the ordered arrays the interparticle distance was ≥ 1 μm, which was considerably greater than the particle diameter (245 nm). The observed ordering could be attributed (i) to a two-dimensional Kirkwood-Alder transition or (ii) to a combination of the electrostatic repulsion and the powerful attraction due to the capillary immersion force (Chapter 7); the latter could appear if during the structuring the particles have touched the substrate, as it is in Fig. 7.1b.

Evidence for clustering of silica particles (300 nm in diameter) at air-water interface was reported by Hurd and Schaefer [96]. The ionic strength of the electrolyte dissolved in the aqueous phase was high enough to limit the range of action of the electrostatic repulsive forces below 1 nm. Under these conditions irreversible dendritic aggregation was observed with particles apparently in direct contact. The bonding was attributed to the van der Waals forces.

Similar experiments with particles at air-water interface were carried out by Onoda [97]. He used larger monodisperse polystyrene latex spheres with size from 1 to 15 μm in diameter. The ionic strength of the aqueous solution was 0.02 M. With the smaller particles (1 μm) little clustering was evident. With the 2 μm particles formation and disassembly of transient 2D aggregates was noticed. With the larger particles, of diameter 5, 10 and 15 μm, irreversible clustering into 2D aggregates was observed. By means of the DLVO theory the depth of the secondary minimum is estimated to be 0.2, 1, 5 and 10 kT (with Hamaker constant A_H = 5×10^{-21} J) for particles of diameter 1, 2, 5 and 10 μm, respectively, which agrees well with the experimental evidence. Although the weight of a single particle is small and cannot create interfacial deformation, the weight of larger particle clusters can bend the interface and give rise to capillary flotation forces between the 2D aggregates [97].

Kondo et al. [98] investigated the 2D aggregation of monodisperse spherical silica particles on the surface of benzene. The experiments included two stages: (i) formation of particle clusters at the air-liquid interface under the action of the van der Waals forces; (ii) formation of ordered domains during the drying of the 2D particle structures on a mica substrate. At the second stage case the capillary immersion forces were operative.

Heki and Inoue [99] observed the formation of 2D ordered arrays of μm-sized crystals of silver bromide floating at air-water interface – see Fig. 12.1. Such ordering of microcrystals was aimed at improving the quality of photographic materials. Initially the microcrystals, which are hydrophobic, have been dispersed in water with the help of gelatin. The ionic strength of the solution was low to prevent coagulation in the bulk. Next, the gelatin was removed by washing with distilled water and the microcrystals emerge at the water-air interface. There they form 2D structures, separated by areas of bare interface. As discussed in Chapter 12, the latter fact suggests that some attractive force has collected the floating microcrystals. This could be the Lucassen's [94] lateral capillary force, the van der Waals and hydrophobic interactions, or their combination.

On molten steel surfaces a strong long-range attraction, which can extend to tens of micrometers, was clearly observed to operate between floating solid particles and to collect them into clusters [100,101]. Such a long-range interaction cannot be attributed to the van der

Waals force [100]. Later estimates [101] showed that most probably this interparticle attraction is a manifestation of the lateral flotation force (see Chapter 8).

13.1.4. FORMATION OF PARTICLE 2D ARRAYS IN ELECTRIC, MAGNETIC AND OPTICAL FIELDS

The electrophoretic deposition method provides another tool for assembly of charged colloidal particles at the surface of an electrode. In the experiments of Giersig and Mulvaney [102,103] citrate- and alkanethiol-stabilized gold particles (samples of average diameter 3.5, 14.1 and 18.5 nm), as well as latex particles of diameter 440 nm, were electrophoretically deposited onto carbon-coated copper grids. A conventional dc power supply was used to generate the applied voltage. After deposition was complete, the copper grid was removed, while the electrodes were still polarized to prevent the occurrence of any desorption of colloid particles. The polarization was then switched off and the solvent in the remaining thin film was allowed to evaporate; finally, the coated grids were examined by electron microscope and ordered 2D domains were observed. The particle agglomeration into clusters evidenced that some attractive surface force must exist between the adsorbed gold particles [102]; it could be attributed to the van der Waals attraction since the Hamaker constant of gold across water is rather high: $A_H = 3 \times 10^{-19}$ J. On the other hand, for the latex particles A_H is almost 100 times smaller; one possible explanation for their ordering is the occurrence of a Kirkwood-Alder transition in a dense population of electrophoretically deposited latex spheres. Alternatively, the observed ordering could be attributed to the action of the capillary immersion force (Fig. 7.1) during the drying of the deposited film.

The electrophoretic deposition of latex and silica particles has been examined in Refs. [104-108]. In some of these studies [105,108] a transparent electrode of conducting glass (indium-tin oxide, or tin oxide) was used to observe directly the process of particle assembly. The deposited particles were seen to spontaneously assemble into clusters, which further grow into ordered domains. In other words, there is a clear evidence about the existence of a lateral attraction between the deposited latex particles [105,108]. It cannot be the van der Waals force (the Hamaker constant is too small), neither it can be the lateral immersion force (the particles do not protrude from a fluid interface). In Ref. [105] it is hypothesized that this attractive interaction is caused by electro-hydrodynamic effects arising from the charge

accumulation near the electrode due to the passage of ionic current. In our opinion, the charged dielectric latex particles certainly disturb the electric double layer formed in a vicinity of the electrode; the overlap of the disturbances around two deposited particles could produce interaction between them. This effect calls for additional investigation.

Not only electric, but also magnetic field was used to produce 2D arrays of colloidal particles. Hexagonally packed 2D arrays and chain-like clusters of polystyrene latex particles ("magnetic holes") were formed when a magnetic field was applied to ferrofluids such as Fe_3O_4, iron or cobalt, and the pattern was numerically simulated by using the Monte Carlo method [109,110]. Dimitrov et al. [111] investigated experimentally 2D arrays of polystyrene beads, containing a ferrite core of Fe_3O_4 and γ-Fe_2O_3, formed at air-water and glass-water interfaces. Takahashi et al. [112] developed a theoretical model describing the forces acting on the particles. The computer simulations reproduced the observed hexagonally aligned 2D patterns, including the interparticle distance and the time of array formation. It was established that the major role is played by the magnetic force and the monopole electrostatic repulsion between two particles; on the other hand, the contribution of the lateral capillary forces and the electrostatic dipolar repulsion were found to be negligible for this experimental system [112].

Finally, it was found experimentally that intensive optical (electromagnetic) fields can cause ordering of microscopic dielectric objects into 2D arrays [113,114]. Two principles of particle organization have been proposed [114]. Firstly, the dielectric particles are ordered in direct response to the externally applied standing wave optical fields; this is the same mechanism, which provides trapping (levitation) of dielectric objects into gradients of optical fields, as established by Ashkin [115] and others [116]. Secondly, the external optical fields can produce interactions between dielectric particles (due to oscillating optically induced dipoles), which can also result in the creation of complex structures [113,114]. In this way "optical crystallization" of polystyrene spheres (3.4 μm in diameter) was experimentally achieved with the help of an argon ion laser delivering power up to 10 W at wavelength 514.5 nm.

13.1.5. 2D ARRAYS OBTAINED BY ADSORPTION AND/OR LANGMUIR-BLODGETT METHOD

Particles or macromolecules can adsorb spontaneously at a given interface. When the energy gain accompanying the adsorption is large enough, the adsorption layer becomes dense and the particles acquire hexagonal packing, i.e. a 2D array is formed. On the other hand, if the obtained adsorption monolayer is not dense, it can be compressed by the movable barrier of a Langmuir trough, which is suitable for handling monolayers from insoluble (or slightly soluble) molecules or colloid particles. The latter method was used by Goodwin et al. [117] to form 2D ordered arrays of latex particles, which were further transferred onto glass slides using the Langmuir-Blodgett approach, see e.g. Ref. [118]. This method was applied also by Fendler and coworkers to prepare particulate mono- and multilayers from surfactant stabilized nanosized magnetite crystallites [119], from cadmium sulfide clusters [120], from silver, platinum and palladium nanocrystallytes [121,122], and from ferroelectric lead zirconium titanate particles [123]. The same method can be applied to form 2D arrays of proteins, see e.g. Refs. [118, 124, 125].

The above experimental approach can be extended to particulates or macromolecules which do not adsorb at the interface itself, but which can bind to some appropriate pre-spread adsorption monolayer. Fendler et al. have used this version of the method to grow various nanocrystallites below adsorption monolayers; for review see Refs. [126,127]. Lipid adsorption monolayers and liposomes are found to be suitable substrates for the growth of two-dimensional crystals of proteins by adsorption from solutions [128-133]. Muratsugu et al. [134-137] have developed a method for preparation of 2D arrays of proteins (immunoglobulins) on a plasma-polymerized allylamine film covered on a silver plate; such arrays find biomedical application as immunoassays or immunosensors.

Yoshimura et al. [138] achieved formation of well ordered 2D arrays of proteins by injection of protein solution into an aqueous subphase that had a higher density and surface tension than the protein solution (solutions of 2 % glucose, 0.15 M NaCl and 10 mM $CdSO_4$ at pH = 5.7 gave the best results). The buoyancy made the injected drop of protein solution to rise and to spread quickly on the liquid-air interface. Firstly, the proteins that reached the interface unfolded instantaneously and formed a continuous film. Secondly, new-coming protein

molecules adsorbed below the latter continuous film and formed ordered 2D arrays of intact proteins [138].

The next sections of this chapter are devoted to a more detailed description of the methods and mechanisms for production of 2D arrays of proteins and particulates in liquid films under the action of the lateral capillary forces and evaporation-driven flow of the fluid.

13.2. 2D CRYSTALLIZATION OF PROTEINS ON THE SURFACE OF MERCURY

13.2.1. THE MERCURY TROUGH METHOD

3D protein crystals are used to establish the tertiary structure of these macromolecules; for that purpose hundreds of proteins have been crystallized [139-145]. In addition, 2D protein crystals are used for electron microscope crystallography [146-148]. When large 2D crystals of good quality are obtained, the tertiary structure of the protein can be determined by image analysis of the electron micrographs [149-152]. Moreover, as mentioned in the beginning of this chapter, 2D arrays of proteins and other nanoparticles represent considerable practical interest for design of nano-technological devices, which are a possible step towards a future high technology at the macromolecular level.

Yoshimura et al. [32] developed a method for 2D crystallization of proteins by spreading a drop of concentrated protein solution on the surface of mercury. There are three reasons to chose mercury as a substrate: (i) its surface is perfectly flat because mercury is liquid (no surface roughness); (ii) the protein suspensions spontaneously spread on the surface of mercury to form a very thin and stable wetting film, in which the two-dimensional crystallization of the protein is accomplished; (iii) in contrast with the methods using localized adsorption [128-133] the protein molecules are not immobilized in adsorption cites; thus they can adjust their location and orientation, which results in the formation of larger well-ordered domains (Fig. 13.1). Two-dimensional crystals of many proteins have been obtained using this method, see Table 13.1.

The 2D-crystallization of proteins is carried out in a mercury trough with a special design [32], see Fig. 13.2. It provides all necessary conditions to create and maintain clean mercury surface, which turns out to be of crucial importance. First of all, the mercury trough is closed

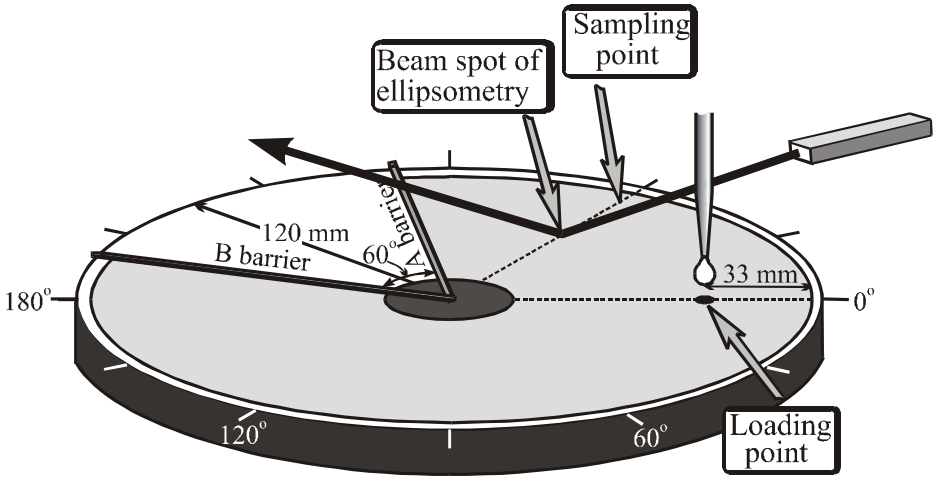

Fig. 13.2. Schematic view of the mercury trough: with the help of the mobile barriers "A" and "B" the mercury surface can be compressed, expanded and cleaned. The surface properties are monitored by ellipsometer. By means of a syringe a drop of protein solution is loaded, and after its spreading sample of the formed film is taken by pressing gently a carbon coated copper grid to the mercury surface.

in a chamber filled with pure oxygen (99.99%). The two rotating barriers (Fig. 13.2) are used to create a new mercury surface and to collect the possible interfacial contamination in a narrow sector; the contaminated surface is removed by ejection of the interfacial layer with the help of a Teflon capillary connected to a vacuum pump. The interfacial cleanness is controlled by measurement of the mercury surface tension by means of the Wilhelmy plate method; an amalgamated platinum plate is used for that purpose [32]. In addition, the cleanness is controlled by means of ellipsometric measurements, which give also the thickness of the spread protein layer [32,153].

The composition of the atmosphere in the chamber with the mercury trough is also important. Experiments with helium, nitrogen and oxygen have been carried out [32]. It turns out that the 2D crystallization of proteins is successful only in the presence of oxygen atmosphere, which provides a uniform spreading of the protein solution on mercury. This is attributed to physical adsorption of oxygen molecules on the mercury surface, which makes it more hydrophilic [154]. The humidity of the atmosphere in the chamber also turned out to be important. In a humid O_2 atmosphere (relative humidity below 50 %) the protein formed an amorphous monolayer rather than an ordered crystal [154]. The best 2D crystals were obtained if the atmosphere before the spreading was 100 % dry oxygen, without water vapors. The effect of

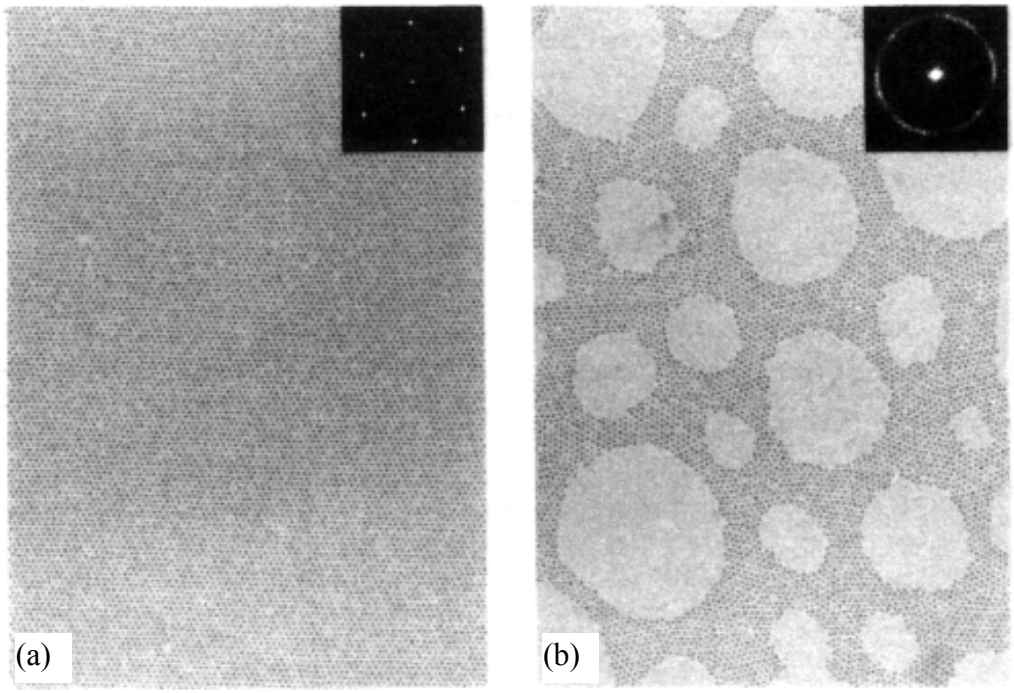

Fig. 13.3. Electron micrograph of 2D arrays of ferritin obtained by Yamaki et al [153] in a mercury trough by spreading of (a) 2μL and (b) 10 μL suspension drops, each of them containing the same amount (0.4 mg) ferritin in the presence of glycerol. The insets show first order diffraction patterns.

humidity on the 2D crystallization is related to two factors, both of them decelerating the spreading and drying of the protein solution: (i) adsorption of water on mercury decreases the spreading coefficient [118]; (ii) the rate of evaporation decreases in humid atmosphere.

13.2.2. EXPERIMENTAL PROCEDURE AND RESULTS

In the experiments [153] a sector of the mercury surface of area 430 cm^2 was used setting the angle between the two radial barriers (Fig. 13.2) equal to 300°. In each experiment a droplet of protein solution, of volume between 2 and 10 microliters, was placed on the mercury surface. The spreading of the droplet is very fast; it takes less than 1 s. To improve the spreading 0.11 M NaCl was added to the protein solution. Addition of either glucose or glycerol improves the spreading more than the addition of NaCl [153]. Moreover, the glucose or glycerol protects the protein molecules from denaturation upon contact with the mercury surface. After 2 min. of spreading the dried protein monolayer was transferred to a carbon film

(supported by a copper grid) by gently attaching it to the mercury surface. If necessary, the specimen could be stained with 1 % uranyl acetate. Finally, the samples were analyzed by transmission electron microscopy (TEM).

Figure 13.3 shows two micrographs of 2D arrays of the protein ferritin spread in the presence of glycerol. Some samples (Fig. 13.3a) show almost perfect hexagonal 2D crystals. Other samples (Fig. 13.3b) show the formation of "2D foam", that consists of dispersed empty zones surrounded by interconnected domains of ordered protein monolayer. The absence of separate protein molecules dispersed in the empty zones evidences for the existence of some attractive force between the protein molecules, which tends to keep them together. To reveal the nature of this force experiments with various nanoparticles have been carried out in the mercury trough [39], see Section 13.5 for more details.

Two-dimensional crystallization of many proteins has been attempted in the mercury trough. One-third of the trials led to obtaining of satisfactorily ordered protein 2D arrays; they are listed in Table 13.1, where the molecular weight of the protein, the symmetry of the obtained 2D crystal and the experimental diffraction order are also listed. The 2D crystals denoted by asterisk (*) are formed by using the alternative glucose-solution-method [138]. The proteins are not highly symmetric molecules; consequently, the crystal symmetry is often P1 (Table 13.1). On the other hand, the hexagonal lattice is a natural form of closely packed globular particles and it is actually the lattice observed with various protein samples tested until now [155]. Micrographs, like Fig. 13.3b, reveal that the close packing is not a result of high protein density, but more likely of the attractive force between the protein molecules.

The successful results obtained with the mercury trough stimulated further research on the mechanism, driving force and kinetics of the two-dimensional crystallization in liquid films. The major results are described in Sections 13.3 – 13.7.

It is worthwhile noting that, except mercury, there is another metal, gallium, which is liquid at body temperature (more precisely, above 29.8°C). The results of the first attempts for crystallization of ferritin on gallium surface were recently reported [156]. Other liquid substrate attempted for protein 2D-crystallization is perfluorinated oil, see Ref. [37] and Section 13.4.1 below.

Table 13.1. Two-dimensional (2D) crystals of proteins obtained by means of the mercury trough method; 2D crystals obtained using the glucose-solution method [138] are denoted by asterisk (*).

Protein	Size (kDa)	Crystal symmetry	Diffraction order	Reference
Chaperonin (from thermophilic bacterium)	420	P1	4	[157]
Holo-ferritin (horse)	400	P3	6; 7*	[32,153]
Apo-ferritin (horse)	400	P3	6	[158]
Apo-ferritin (human)	400	P3	6	[159]
H^+–ATPase (TF1 - PS3)	340	P1 (P3)	4	[31,32]
H^+–ATPase (TF1 - Sulfolobus)	400	P1 (P3)	3	[151]
$\alpha_3\ \beta_3$ (PS3)	280	P3	3	[31]
LDH (thermophilic bacterium)	300	–	2	[160]
Proteasomes (thermophilic bacterium)	300 ?	–	3*	[138]
C-reactive protein (human)	118	–	3*	[161]
Myosin S1 (rabbit skeletal)	100	–	0	[160]
Troponin (rabbit skeletal)	68	–	0	[160]
Tropomyosin (rabbit skeletal)	64	–	0	[160]
Streptoavidin	60	P2	3	[160]
Cytocrome b_{562}	20	–	0	[160]
Methallothionetin (rabbit liver)	8	–	0	[160]
H^+–ATPase F0-F1 (PS3)	500	P1(P3)	3	[155]
LP ring, flagella motor (salmonella)	1300	P3(P6)	9	[162]
Na^+, K^+-ATPase (dog kidney)	120	–	0	[155]
Cytocrome P450	54	–	0	[155]

13.3. DYNAMICS OF 2D CRYSTALLIZATION IN EVAPORATING LIQUID FILMS

13.3.1. MECHANISM OF TWO-DIMENSIONAL CRYSTALLIZATION

Many methods for obtaining two-dimensional ordered arrays of proteins and colloidal particles involve a deposition and/or spreading of a suspension droplet over a substrate, followed by evaporation of the solvent (usually water). Examples are the mercury trough method described in Section 13.2, the method used to crystallize viruses [21-23]; the negative staining–carbon film procedure [24-30], the formation of 2D arrays on graphite and mica [63-65], ordering of latex, silica and other colloidal particles on various substrates [59-62, 163-167].

Many of the works on 2D array formation describe the applied procedure and the final result of ordering. However, the mechanism and stages of the process of ordering demand a special investigation, which can reveal the forces and factors governing the array formation. Such a study has been carried out by Denkov et al. [33,34], who undertook direct microscopic observations of the 2D crystallization of μm-sized latex spheres. The cell used in this study is depicted in Fig. 13.4. In the experiments a drop of latex suspension spreads over the accessible area of a hydrophilic glass substrate encircled by a Teflon ring of inner diameter 14 mm. The inner wall of the ring is cut slantwise (the inset in Fig. 13.4) to ensure the formation of slightly concave liquid meniscus, which favors the formation of larger 2D ordered

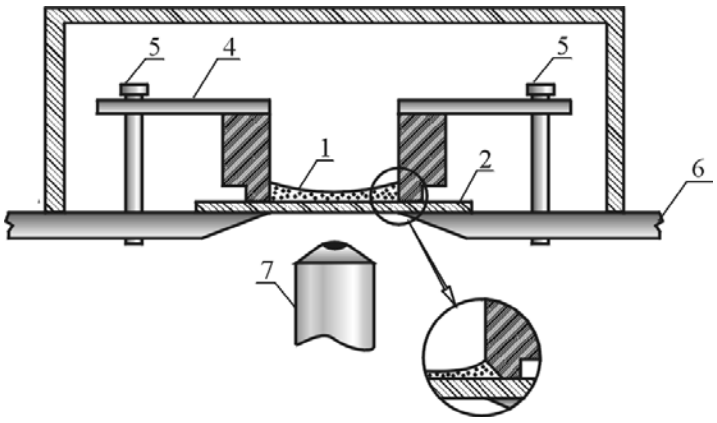

Fig. 13.4. Sketch of the experimental cell used by Denkov et al. [33] to produce particle 2D arrays in a liquid layer with concave surface (1) over a glass substrate (2) encircled by a hydrophobic (Teflon) ring (3), which is fixed with the help of a brass plate (4) and screws (5) to the microscope table (6); (7) is microscope objective.

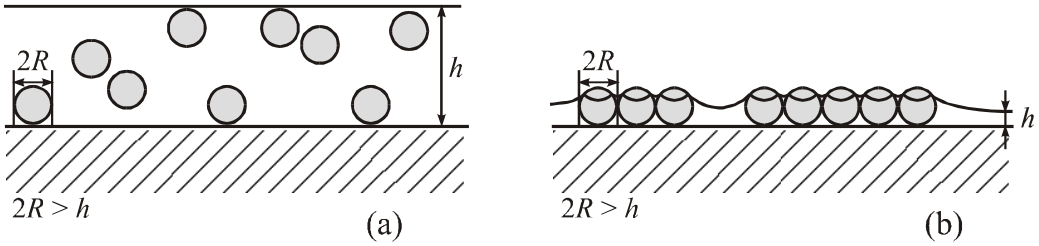

Fig. 13.5. Schematic presentation of the process of 2D ordering of suspension particles in an evaporating liquid layer on a solid substrate: (a) Brownian motion of the particles in a thick layer (b) after the particle tops protrude from the liquid layer, lateral capillary forces appear and cause aggregation of the particles.

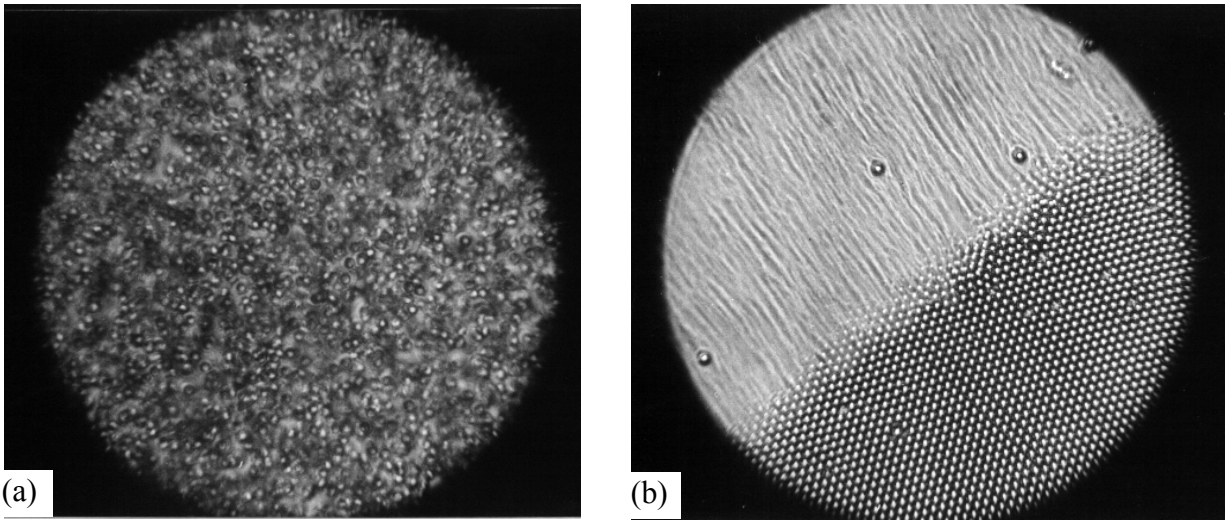

Fig. 13.6. Photographs taken by Denkov et al. [33] of two consecutive stages of the process of 2D array formation from latex particles (1.7 μm in diameter): (a) Brownian motion of the particles in a 10 μm thick aqueous layer; (b) growth of a hexagonal array – the tracks of particles moving toward the ordered phase are seen.

arrays. The events happening in the experimental cell were observed from below by means of an optical microscope. The stages of the 2D array formation, as observed in Refs. [33,34], are described below.

At the initial stage of the experiments the liquid layer has a thickness of about 100 μm. The microscopic observations show that the latex particles (of diameter 1.70 μm) are involved in intensive Brownian motion, see Fig. 13.5a and 13.6a. As the layer thickness gradually decreases owing to the water evaporation, the particle concentration increases, the particles come closer and closer and often collide with each other. However, no aggregation or irreversible particle attachment to the glass surface is noticed.

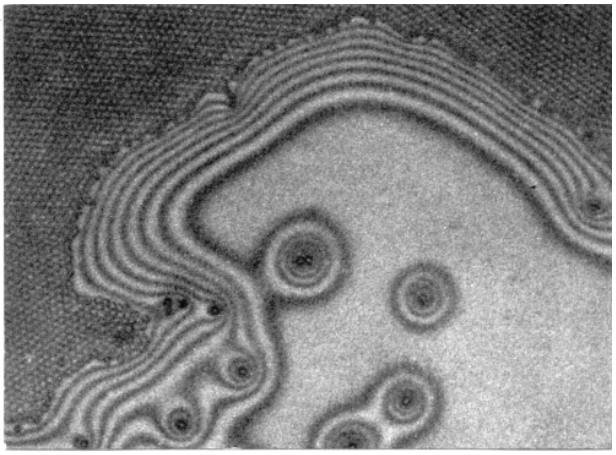

Fig. 13.7. The boundary between an ordered particle monolayer (the dark zone) and a "lake" (water layer free of particles - the bright zone); every transition from dark to bright interference band corresponds to a 102 nm difference in the water layer thickness; photograph from Ref. [33].

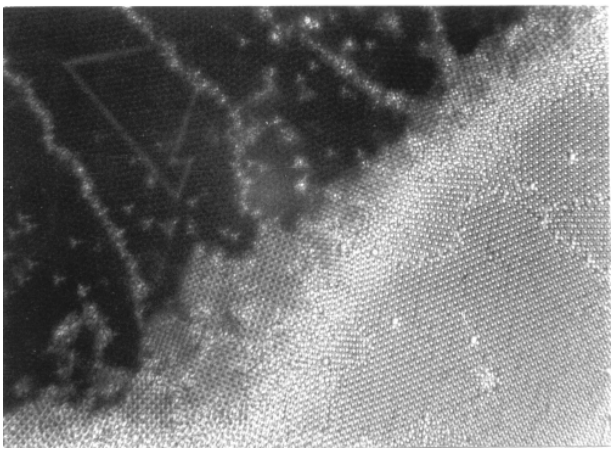

Fig. 13.8. A hexagonal monolayer (bright, lower right) and a hexagonal bilayer (dark, upper left) from ordered 1.7 μm latex spheres; particles packed in a square lattice are seen in the transition zone; photograph from Ref. [33].

When the layer thickness becomes c.a. 10 μm, one can see the appearance of concentric Newton interference rings in the central zone of the wetting film, where the thickness is the smallest. From the number and brightness of the respective rings one can estimate the local thickness of the wetting film (monochromatic light of wavelength λ = 546 nm has been used) [33,34]. As the thickness continues to decrease, the latex particles remain in Brownian motion. Occasionally one can observe that the tops of few larger particles (having diameter greater than the average) protrude from the aqueous film; no movement of these particles is noticed after that. Such particles are found eventually to create defects in the 2D crystal.

When the film thickness in the central zone of the cell becomes about the particle diameter, one observes the formation of a ring-shaped narrow zone (nucleus) of closely packed particles over the middle of the glass substrate, Fig. 13.5b. The ordered region is surrounded by a thicker liquid film, in which the volume fraction of the particles is lower than 10 % [33,34]. This is the beginning of growth of a two-dimensional crystal, which suddenly changes the pattern of the particle motion. The particles in the thicker layer rush towards the ordered zone and upon reaching the boundary of the array they are trapped in it (Fig. 13.6b). Thus the front of the 2D crystal advances with time in a radial direction, from the center of the

substrate toward the ring wall. Inside the ordered array of hexagonal packing sometimes one can observe "lakes" representing regions free of particles, where the glass substrate is covered only by an aqueous layer. Counting the number of the interference fringes in a vicinity of the shore of such a lake (Fig. 13.7) one can estimate that the thickness of the water layer at the boundary of the 2D array is slightly below the particle diameter (1.7 μm) [33,34].

When the radius of the ordered domain becomes about 3-4 mm and approaches the boundary of the experimental cell, one often observes a transition from monolayer to bilayer (Fig. 13.8). Usually at the boundary between *hexagonal* monolayer and bilayer one observes small domains of particles packed in square lattice (Fig. 13.8). In some experiments multilayers have been obtained with the following sequence of layers: 1Δ–2❑–2Δ–3❑–3Δ–⋯ [33,36]; here the ciphers correspond to the number of layers and the symbols mean hexagonal (Δ) or tetragonal (❑) packing of the particles. This order exactly coincides with the phase diagram calculated and observed by Pieranski et al. [86,87] for colloid particles confined in a narrow wedge-shaped gap between two solid plates.

The experimental study of the influence of various factors on the occurrence of the two-dimensional crystallization is helpful for revealing the driving forces behind the observed events. In Ref. [33] the effect of *particle concentration* was examined. Although the concentration was varied over one order of magnitude (from 0.25 to 2.5 wt %), no substantial difference in the occurrence of the 2D crystallization was established. At the lower concentrations a "2D-foam" structure, i.e. large zones free of particles formed amidst interconnected bands of ordered particles, were often observed (Fig. 13.9). Note the resemblance between Figs. 13.9 and 13.3b. On the other hand, when the particle concentration was higher, larger areas were covered by bilayers.

Other factor examined in Ref. [33] is the *electrolyte concentration*, which affects the electrostatic interactions between the negatively charged latex particles. By electrophoretic measurements it was found that the addition of 5×10^{-4} M $BaCl_2$ in the suspension alters the particle ζ-potential from −106 to −53 mV. As a result, at the stage of Brownian motion (Fig. 13.6a) a pronounced tendency for formation of transient aggregates (of 2-5 particles) was observed, which could be attributed to the screened electrostatic repulsion. The aggregation

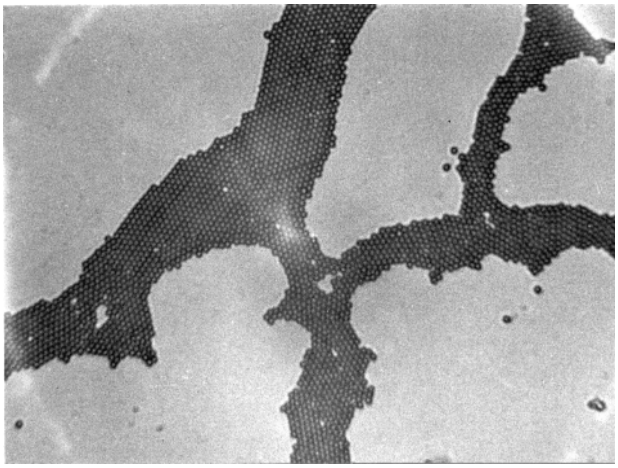

Fig. 13.9. A dried "2D-foam" structure of ordered latex particles (diameter 1.7 μm) obtained in the presence of 0.008 M SDS at a low particle concentration; photograph from Ref. [33].

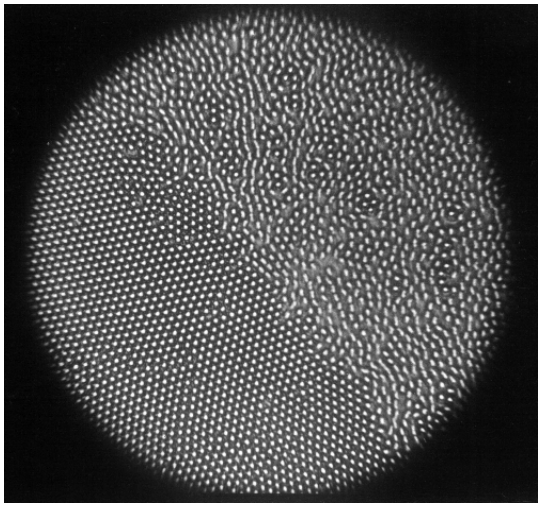

Fig. 13.10. Photograph from Ref. [34] of the growth of a 2D array from latex spheres in the presence of glucose, which decreases the rates of water evaporation and particle motion: the tracks are shorter as compared to those in Fig. 13.6b.

was reversible and the process of ordering followed the same pattern as in the absence of $BaCl_2$. Similar was the effect of addition of 0.01 M NaCl. On the other hand high electrolyte concentration (say $BaCl_2$ above 2×10^{-3} M) brings about coagulation in the bulk of the latex suspension and 2D crystallization is not observed.

It has been established [33] that the *water evaporation rate* is an important factor for the 2D array formation. The evaporation rate can be changed by varying the volume of the air space above the liquid layer, or by creation of a vertical temperature gradient [37]. For example, the reduction of the volume of the gas space from 250 to 1 cm^3 resulted in a 10-times decrease of the rate of all processes, including the speed of the directional motion of the particles (Fig. 13.6b) and the rate of array growth. The decrease of the volume caused formation of larger ordered domains and larger areas covered with bilayer. A further increase of humidity of the air in the cell leads to complete stopping of the process of ordering and even to disintegration of the ordered clusters and restoration of the chaotic particle motion [33].

Note that the evaporation rate can be slowed down also by the addition of anionic (SDS) or cationic (HTAB) *surfactant*, which form a dense adsorption layer on the liquid surface, which

decelerates the evaporation. The addition of cationic surfactant has the disadvantage to create irreversible attachment of the negatively charged latex particles to the negatively charged glass substrate, which eventually causes many defects in the obtained 2D array [33]. In other experiments *glucose* was added to the suspension [34]; it also decreases the kinetics of 2D array growth (Fig. 13.10) because of reduction of the evaporation rate and increase of the viscosity of the aqueous phase.

The shape of the surface of the liquid layer also influences the occurrence and the result of the 2D crystallization. In the experimental cell depicted in Fig. 13.4 a slightly *concave* meniscus is formed and the 2D crystallization starts from the central (thinner) part of the liquid layer. This geometry leads to the formation of large ordered particle monolayers or bilayers, see Fig. 13.11. On the other hand, if a drop of the latex suspension is placed on the same glass plate, but without surrounding Teflon ring, the drop spreads over a certain area and forms a *convex* meniscus, which meets the glass surface at a contact angle of a few degrees. In this case the thinnest zone of the liquid layer is at the periphery of the drop, where the growth of particle array follows the shrinking of the contact line of the drying drop. In this case a directional motion of latex particles from the center of the drop toward its periphery is observed, which results in the formation of a thick multilayer of particles, see Fig. 13.12. In the central part only a small amount of particles remains and forms small clusters. Large and well ordered arrays were not obtained with convex drops [33].

Similar mechanism of 2D crystallization was established irrespective of the *particle size*: latex particles of diameters 1700 and 814 nm [33], latex particles of diameter 144 and 55 nm [35,36,38], latex particles of diameter 95 and 22 nm, virus and protein of diameters 30 and 12 nm, respectively [39]. First of all, the fact that the addition of electrolyte strongly suppresses the electrostatic interactions without substantial changing of the ordering process, shows that the observed 2D crystallization can be attributed neither to the DLVO surface forces (responsible for the bulk coagulation) [84,95], nor to a Kirkwood-Alder phase transition in concentrated suspensions (a volume restriction effect, see Section 13.1.2). Similarly, the change of the particle concentration does not affect the onset of ordering, whereas with 3D crystals this is the major factor governing the phase transitions. In all experiments [33-38] the

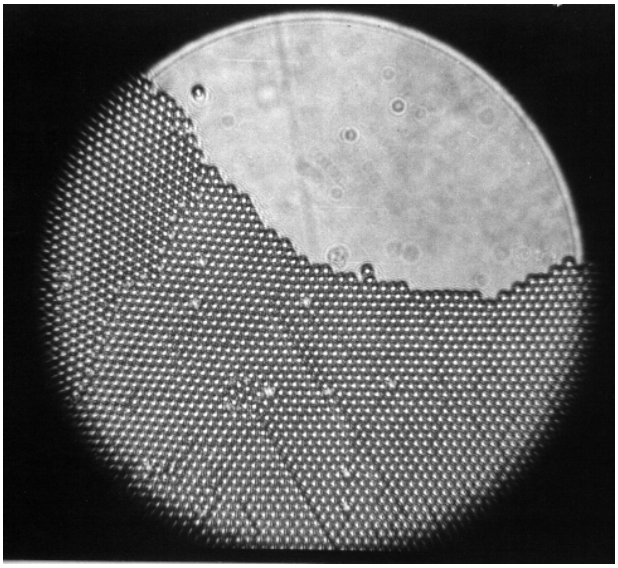

Fig. 13.11. A transition from a dried ordered monolayer to area free of particles (1.7 μm in diameter); photograph from Ref. [33].

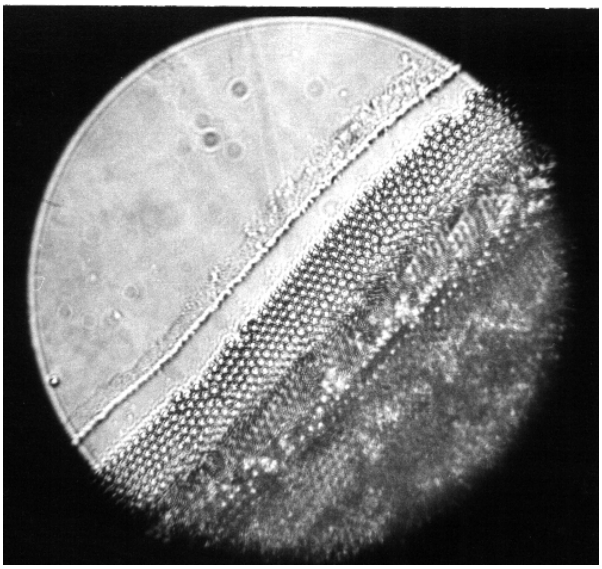

Fig. 13.12. Periphery of a latex suspension drop drying on a glass plate without a surrounding ring; a thick multilayer of particle deposits is formed (lower dark zone); photograph from Ref. [33].

2D array formation starts when the thickness of the water layer becomes approximately equal to the particle diameter and the crystal grows through a directional motion of particles toward the ordered regions. A coexistence of ordered domains and regions free of particles, with a sharp boundary between them, is often observed (Figs. 13.9 and 13.11); the latter fact cannot be explained with the action of repulsive forces alone. Considering the experimental facts the following two-stage mechanism of 2D crystallization was proposed [33,34]:

1) At the first stage, immediately after the protrusion of the particle tops from the liquid layer, the attractive lateral immersion forces collect particles into a "nucleus" of the ordered phase. The immersion force is significant even for nm-sized particles, see Chapter 7 and Fig. 8.3.

2) Once the nucleus is formed, the second stage of crystal growth starts through directional motion of particles toward the ordered array. It is caused by the hydrophilic nature of the surface of the particles: the level of the liquid in the nucleus and in the growing ordered 2D array must be high enough to wet the predominant area of the particle surface and to ensure the formation of a small contact angle particle-water-air, see Fig. 13.13. Therefore, the water

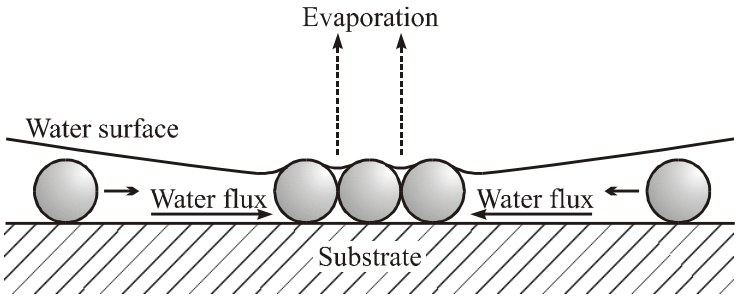

Fig. 13.13. Schematic presentation of the particle assembly process: the water evaporated from an aggregate of hydrophilic particles is compensated by the influx of water from the surrounding thicker liquid layer; the flux brings new particles to the growing 2D array.

evaporated from the 2D array must be compensated by the influx of water from the surrounding thicker liquid layer (Fig. 13.13) in order to keep wet the particles in the ordered domain. This brings about an intensive water flow toward the ordered domains, which carries along suspended particles. Upon reaching the boundary of the array the "newcomers" remain attached captured by the capillary attraction (the immersion force).

The above two-stage mechanism agrees well with numerous experimental data, see Refs. [33-39]. It provides a quantitative theoretical description of the kinetics of 2D crystal growth, which compares well with the experiment; see the next Section 13.2.3.

13.3.2. KINETICS OF TWO-DIMENSIONAL CRYSTALLIZATION IN CONVECTIVE REGIME

An important feature of the mechanism of 2D crystal growth described in Section 13.2.2 is the presence of evaporation-driven *convective* flow, which carries the suspended particles towards the nucleus [33,34]. This convective regime provides a rapid growth and good particle ordering, which makes a big contrast with the *diffusion* limited crystallization [168,169]. The latter is characterized by a relatively low rate and frequent formation of random dendrite (fractal) structures [170,171], like that observed in the processes of ice-growth on a cold glass or formation of snowflakes in the air.

As discussed in the previous section, the kinetics of convective growth depends on the evaporation rate and the shape of the liquid meniscus (concave or convex), which in turn depend on the specific construction of the experimental cell.

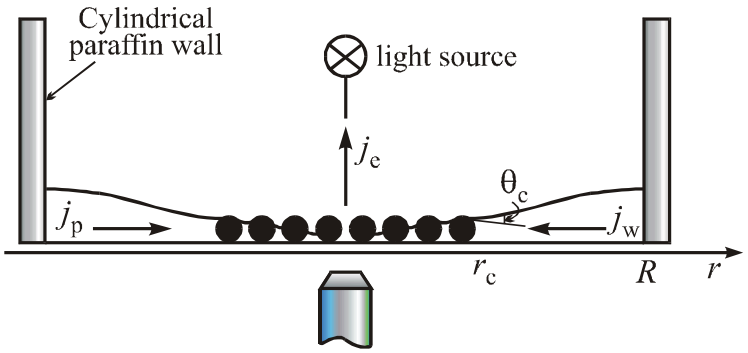

Fig. 13.14. Sketch of the experimental cell with paraffin wall used by Dushkin et al. [35] to produce 2D arrays of sub-μm polystyrene latex spheres. The processes in the cell are recorded by a video-microscope system. The evaporation flux j_e drives convection fluxes of water, j_w , and particles, j_p , toward the growing array.

To study the kinetics of 2D crystallization Dushkin et al. [35] used an experimental cell depicted in Fig. 13.14. It was made by piercing a circular hole of diameter 2 mm across a paraffin block, which was then sealed to a hydrophilic transparent plate (glass or mica) representing the substrate for 2D crystal growth. The sealing was achieved simply by a local melting of the paraffin surface (at about 70°C). In the experiments the cell was loaded with 1 microliter aqueous suspension of polystyrene latex particles of diameter 144 nm (±2 nm) at particle volume fraction $\phi = 0.001$. The upper side of the cell was kept open allowing the water to evaporate at constant temperature 20°C (±2°C) and relative humidity 30 % (±3 %). The crystal growth was recorded by microscope and video-camera.

The observed consequence of events is similar to that described in the previous section. Owing to the water evaporation the liquid layer in the cell thins; at a certain moment a plane parallel liquid film is formed in the central zone, which can be distinguished by the appearance of interference rings around its periphery (Fig. 13.15a). The ordering starts from the center of the cell, where the film is the thinnest and the protrusion of the particle tops from the liquid first happens. A "2D-foam" structure with many empty areas is observed in the central zone, see Fig 13.15b, which is taken about 1 min. after the beginning of the experiment; the boundary (of elliptic shape) between the array and the surrounding thicker liquid layer is also seen in Fig. 13.15b. The area occupied by the particle array expands with time. Fig. 13.15c shows the final result, after evaporation of the whole amount of water. Because of some instabilities the central

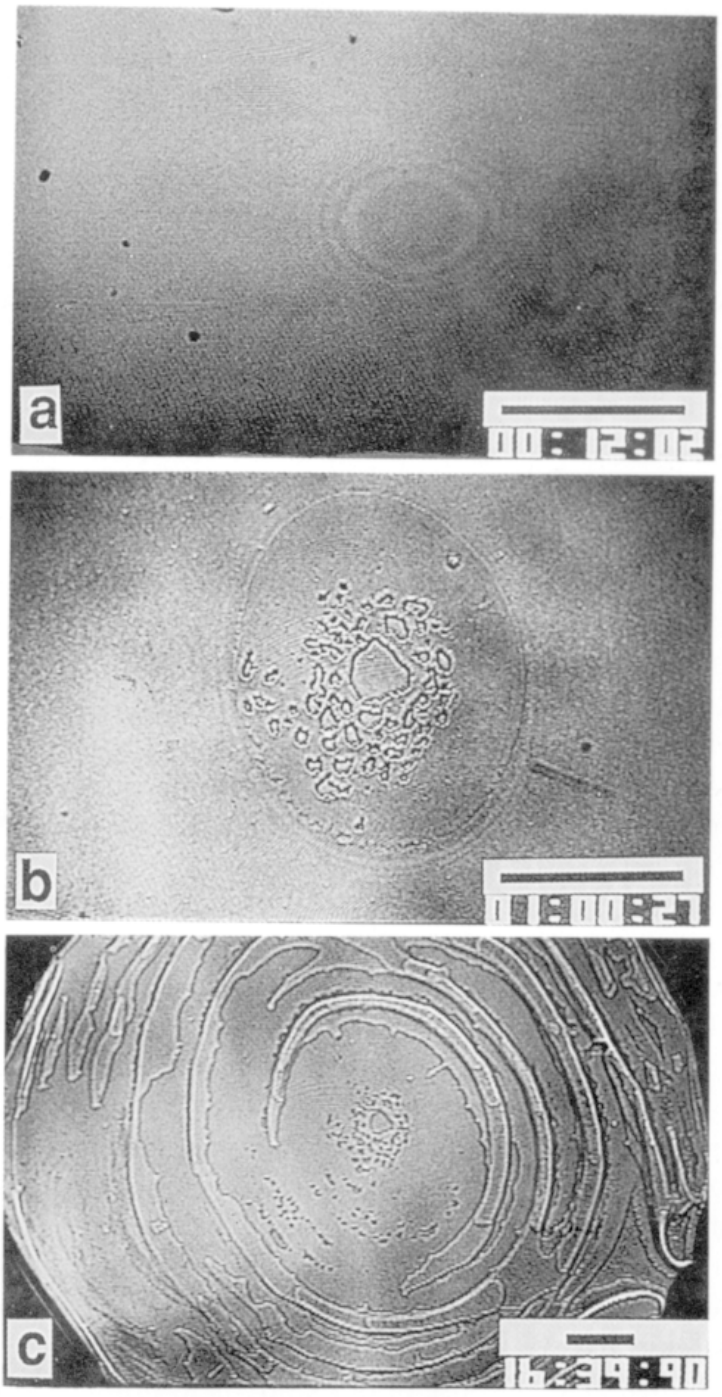

Fig. 13.15. Consecutive stages of 2D array growth video-recorded by Dushkin et al. [35]: (a) interference fringes (light wavelength 540 nm) from a thinning liquid film prior to the array formation; (b) initial stage of growth of 2D array of latex particles (diameter 144 nm); the array has "2D-foam" structure with empty places; (c) final view of the whole area (3.14 mm^2) covered with radial domains of particle monolayer, separated by multilayered ridges and/or empty zones. The bars correspond to 200 μm.

zone is surrounded by alternating multilayer and monolayer rings. During the formation of such a multilayered ring one observes a decrease of the speed of the boundary between the array and the thicker liquid layer. The reasons for this instability are discussed at the end of this section. The area between the multilayered rings is occupied by a hexagonally packed particle monolayer like that in Fig. 13.11; this was established by means of electron microscopy [35]. To describe quantitatively the kinetics of growth, let us introduce the fluxes of water molecules and colloidal particles at the boundary of the growing 2D array:

$$j_w = c_w v_w , \qquad j_p = c_p v_p = c_p \beta v_w \tag{13.2}$$

Here v_w and v_p are the velocities of water and particles at the boundary array-meniscus; the coefficient β accounts for the fact that the velocity of the particles convected by the flow could be somewhat different from the hydrodynamic velocity of water, $v_p = \beta v_w$; c_w and c_p denote the concentrations of water and particles (number of molecules or particles per unit volume). The number of particles joining the array per unit time is [35]

$$\frac{dN_p}{dt} = j_p A_h \tag{13.3}$$

where A_h is the cross sectional area of the periphery of the crystal of thickness h, and t is time. The increase of the number of the attached particles can be related to the increase of the volume of the array [35]:

$$dN_p = \phi_a \frac{d(Ah)}{V_p} \tag{13.4}$$

where V_p is the volume of a colloidal particle, A and ϕ_a are the area of the array and the volume fraction of the particles within it. Further, we notice, that the water flux j_w through the periphery of the array is driven by the evaporation flux j_e of water molecules per unit area of the evaporating surface, A_e, of the array [35]:

$$j_w = j_e \frac{A_e}{A_h} \tag{13.5}$$

The combination of Eqs. (13.2) and (13.5) yields

$$j_p A_h = \beta \frac{c_p}{c_w} A_h j_w = \beta \frac{c_p}{c_w} A_e j_e \tag{13.6}$$

Next, substituting Eqs. (13.4) and (13.6) into the mass balance equation (13.3) one obtains the basic differential equation describing the growth of the ordered area $A(t)$ [35]:

$$\frac{dA}{dt} = \frac{\beta V_{\mathrm{p}} c_{\mathrm{p}}}{\phi_a h c_{\mathrm{w}}} A_{\mathrm{e}} j_{\mathrm{e}} \tag{13.7}$$

Here we have used the fact that between two step-wise transitions the thickness of the array remains constant, h = const.

Further, to obtain quantitative results one has to additionally specify the system. For the experimental cell, used by Dushkin et al. [35] the additional conditions are:

(i) During the process of growth the boundary of the array, the contact line array-meniscus, is (approximately) a circle of radius $r_c(t)$.

(ii) The convection at the boundary array-meniscus is stationary, that is the parameters c_{w}, c_{p} and β, as well as the rate of evaporation j_{e}, can be (approximately) considered as being independent of time.

(iii) Owing to the fast evaporation, the central part of the array has already dried; consequently, evaporation takes place from a circular ring of width b (wet array) situated in a close vicinity of the contact line; in stationary regime b is assumed independent of time [35].

(iv) The defects of the ordered monolayer, such as empty areas and multilayers, cover relatively small area and can be neglected in a first approximation.

The additional conditions (i) and (iii) imply

$$A = \pi r_c^2, \qquad A_{\mathrm{e}} \approx 2\pi r_c b, \qquad (b << r_c) \tag{13.8}$$

The substitution of Eq. (13.8) into Eq. (13.7) yields a simple equation for $r_c(t)$:

$$\frac{dr_c}{dt} = \mathrm{v_c}, \qquad \text{where} \qquad \mathrm{v_c} \equiv \frac{\beta \ j_{\mathrm{e}} V_{\mathrm{p}} c_{\mathrm{p}} b}{\phi_a c_{\mathrm{w}} h} = \frac{\beta \ j_{\mathrm{e}} V_{\mathrm{w}} \phi \ b}{\phi_a (1-\phi) h} \tag{13.9}$$

Here we have expressed the particle and water numerical concentrations, c_{p} and c_{w}, through the volume fractions of the particles in the suspension ϕ; $V_{\mathrm{w}} \approx 30$ Å^3 is the volume per water molecule; $\mathrm{v_c}$ has the meaning of a velocity of advance of the contact line, or a linear rate of

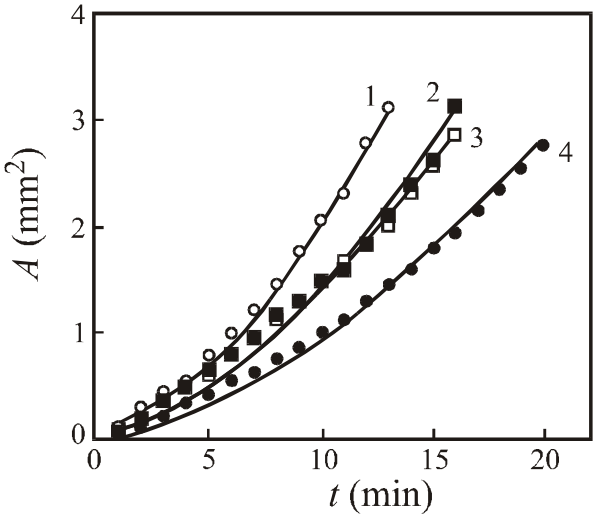

Fig. 13.16. Experimental data for the area, A, of a growing 2D vs. the elapsed time, t, corresponding to 4 different runs (the different symbols). The solid lines are drawn with the help of Eq. (13.10) by the least squares method; results from Ref. [35].

growth of the ordered array. In stationary regime v_c is constant and from Eqs. (13.8) and (13.9) one obtains [35]

$$r_c = v_c t + r_{c0}\,; \qquad A(t) = \left(\sqrt{\pi}\, v_c t + \sqrt{A_0}\right)^2, \qquad A_0 \equiv \pi r_{c0}^2 \tag{13.10}$$

Equations (13.10) predict that in stationary regime the radius of the array r_c increases linearly with time, and the area A of the 2D crystal grows as a quadratic function of time; r_{c0} and A_0 are, respectively, radius and area of the ordered domain formed at the initial stage of 2D crystallization, before the establishment of stationary regime.

Figure 13.16 shows experimental data of Dushkin et al. [35] for $A(t)$ in the case of particle diameter 144 nm; the data agrees well with Eq. (13.9). From the best fits values of v_c from 6.8 μm/s (Curve 4) to 10.7 μm/s (Curve 1) have been calculated. The evaporation flux $j_e = 6.12 \times 10^{17}$ cm^{-2} s^{-1} was measured in an independent experiment, and then the value of the width of the wet zone was estimated to be $b \approx 40$ μm, which seems reasonable [35]. The theoretical model agrees well also with similar data for particles of diameter 55 μm.

Coming back to the multilayers, whose formation has been neglected in the previous theoretical consideration, we should mention that depending on their thickness (number of layers) they exhibit different colors when observed in reflected or transmitted polychromatic light [36]. The most pronounced color effect was observed with multilayers deposited on a

gold-coated glass substrate, see Table 13.2. The colors of the layers from transparent latex spheres are due to light interference at plane parallel films of different thickness. By measuring the wavelengths, at which the reflectance from two neighboring multilayers coincide, it has been established that the particle array has hexagonal packing, which is in agreement with the electronic microscope pictures; see Ref. [36] for details. The same interference method has been applied to establish that the spherical micelles in stratifying foam films are also hexagonally packed [172].

Table 13.2. Interference colors (in reflected light) exhibited by dried multilayers of 55 nm polystyrene latex spheres deposited on gold-coated glass; data from Ref. [36].

number of layers, k	thickness h_k (nm)	color in reflected light	number of layers, k	thickness h_k (nm)	color in reflected light
1	47	ochre	7	277	magenta
2	85	brown	8	316	blue-purplish
3	124	navy blue	9	354	green
4	162	sky blue	10	392	yellow-green
5	201	yellow	11	431	orange
6	239	orange	12	469	red

Finally, we give an idea about the origin of the instability, which causes the appearance of alternatively changing rings of particle monolayers and multilayers (Fig. 13.15c). First, notice that evaporation takes place not only from the drying 2D array, but also from the surrounding liquid layer. Let us denote the volume of the latter by V:

$$V = 2\pi \int_{r_c}^{R} dr \; r\, z(r) \tag{13.11}$$

Here $z(r)$ is the shape of the generatrix of the axisymmetric meniscus encircling the array; R is the radius of the inner cylindrical wall of the experimental cell, see Fig. 13.14. The profile $z(r)$ can be determined by integration of the Laplace equation of capillarity, Eq. (2.24) with $\varphi \equiv \theta$:

$$r \sin\theta = r_c \sin\theta_c + k_1 (r^2 - r_c^2), \qquad k_1 \equiv P_c / 2\sigma \tag{13.12}$$

For small meniscus slope, as it is in Fig. 13.14, with the help of Eq. (13.12) one obtains

$$\frac{dz}{dr} = \tan\theta \approx \sin\theta = k_1 r + r_c(\sin\theta_c - k_1 r_c)/r \tag{13.13}$$

Integrating Eq. (13.13) one determines $z(r)$, and further, substituting Eq. (13.11) one obtains analytical expression for $V = V(r_c)$. For our considerations it is important that the evaporation from the encircling *meniscus* provides an expression for the velocity of the contact line,

$$\mathrm{v_c} \equiv \frac{dr_c}{dt} = \frac{dr_c}{dV}\frac{dV}{dt} \approx -\frac{dr_c}{dV} V_\mathrm{w} j_\mathrm{e} \pi (R^2 - r_c^2) \qquad (b << r_c) \tag{13.14}$$

at the last step we have approximated the evaporating area with $\pi(R^2 - r_c^2)$, which is a good approximation for small meniscus slope. Equation (13.14) expresses the rate of receding of the liquid meniscus, whereas Eq, (13.9) represents the rate of advance of the ordered array owing to the supply of new particles. For a steadily growing 2D array these two rates must coincide. The latter physical requirement determines the local thickness, h, of the particle array: insofar as Eqs. (13.9) and (13.14) must give the same $\mathrm{v_c}$, one obtains

$$\left[\frac{\beta\phi}{\pi\phi_a(1-\phi)}\left(-\frac{dV}{dr_c}\right)\right]\frac{b}{(R^2 - r_c^2)h} = 1 \tag{13.15}$$

One can check that dV/dr_c is not very sensitive to the variation of r_c. With the help of Eq. (13.15) the instability in the 2D crystal growth can be interpreted in the following way:

(i) With the growth of the ordered array the term $(R^2 - r_c^2)$ decreases, see the denominator in Eq. (13.15), which can be compensated by increase of h, i.e. by the formation of a multilayer.

(ii) As experimentally observed [35], when a multilayer is formed the velocity of advance of the contact line decreases, which will certainly result in a shrinking of the width b of the wet 2D array zone because of the advancing front of the dried array.

(iii) Since b and h enter Eq. (13.15) as a ratio (b/h), the decrease of b can be compensated by a decrease of h, that is again a monolayer (and even intermediate zone free of particles) can be formed. The monolayer grows and after a certain time the events are repeated starting from step (i) above.

The above three-step mechanism can be applied to quantify the consecutive formation of monolayers and multilayers (Fig. 13.15c); an adequate description requires to take into account the increase of the particle volume fraction, i.e. $\phi = \phi(t)$, and the variation of the width $b(t)$ of the wet zone.

13.4. LIQUID SUBSTRATES FOR 2D ARRAY FORMATION

13.4.1. FLUORINATED OIL AS A SUBSTRATE FOR TWO-DIMENSIONAL CRYSTALLIZATION

The possibility for application of fluorinated oil (F-oil) as a liquid substrate for 2D array formation was studied in Ref. [37]. Perfluoromethyldecalin (PFMD) was used, which possesses some of the appropriate properties of the mercury substrate (molecularly smooth and tangentially mobile surface, cf. Section 13.2.1) as well as some additional advantages: (i) it is chemically inert and hazardless [173-175]; (ii) it allows the merging and rearrangement of already ordered domains into larger ones; (iii) the formed 2D structures can be gently deposited onto another surface after evaporation of all F-oil and (iv) it is difficult to contaminate the fluorocarbon surface insofar as the common surfactants adsorb poorly at the fluorocarbon-water interface [176].

The physicochemical properties of PFMD are: molecular mass 512.1 Daltons, mass density 1.94 g/cm^3 at 25°C, boiling temperature 141°C, melting temperature –10°C; insoluble in water or liquid hydrocarbons; refractive index 1.315; surface tension 19.2 mN/m; interfacial tension against pure water 53.4 mN/m.

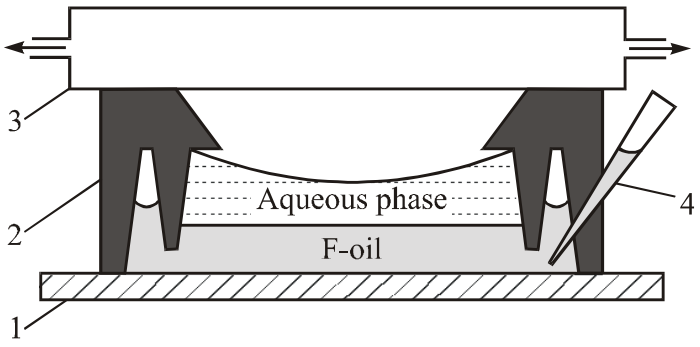

Fig. 13.17. Experimental cell used in Ref. [37] to produce 2D arrays of particles on F-oil substrate: 1- glass plate, 2- Teflon ring, 3- glass container for control of temperature and evaporation, 4- micro-syringe for control of the oil level and the meniscus shape.

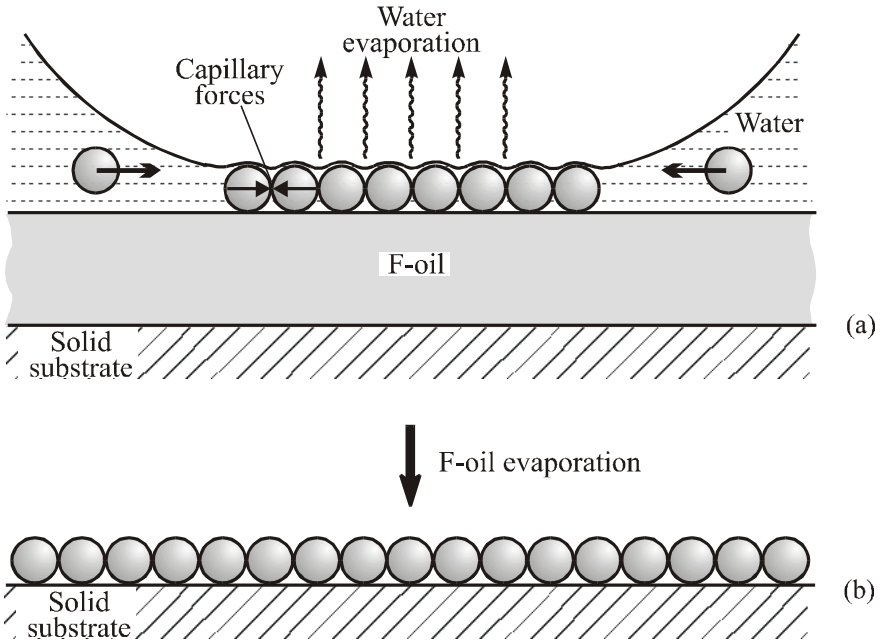

Fig. 13.18. (a) The 2D array nucleation and growth over F-oil substrate are performed under the combined action of attractive lateral capillary forces and an evaporation driven supply of particles; (b) the formed 2D array is automatically deposited on a solid substrate after the consecutive evaporation of the water and F-oil.

The experiments on two-dimensional crystallization have been carried out in a cell depicted in Fig. 13.17. The special cross section ensures attachment of the meniscus of the aqueous layer to the concave corner of the Teflon ring. The bottom of the experimental cell is transparent and allows observations of the processes on the F-oil surface from below, through the F-oil phase. It is possible to control the rate of evaporation from the aqueous layer (and the rate of 2D array growth) varying the temperature of the water circulating through the glass container at the top of the cell. In addition, via sucking or injection of F-oil by a microsyringe one can control the thickness of the aqueous layer spread over the F-oil [37]. To spread drops of aqueous latex suspensions or protein solutions over the fluorinated oil appropriate fluorinated surfactants were used [37]. Best results were obtained with a mixture of the *surfactant* perfluoro-nonylpolyoxyethylene, $C_9F_{19}CH_2CH(OH)CH_2(OCH_2CH_2)_9OCH_3$, and the fluorinated alcohol $C_8F_{17}(CH_2)_2OH$ as a *cosurfactant*. This mixture of surfactant and cosurfactant provided hydrophilization of the F-oil surface and spreading of aqueous layers which were very stable and did not rupture during the experiments with latex particles and ferritin suspensions.

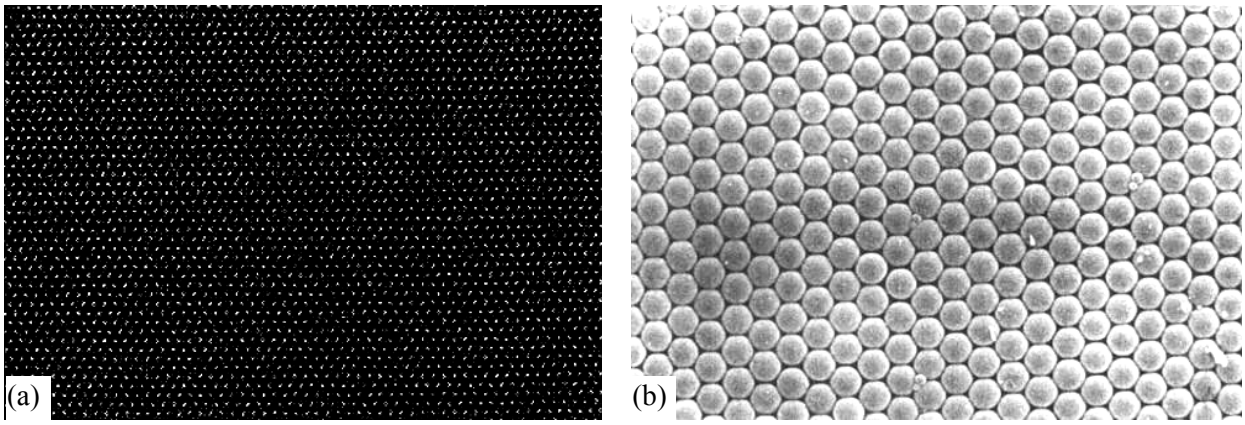

Fig. 13.19. Large, well ordered domains of 1.7 μm polystyrene latex spheres (1.7 μm in diameter) obtained over F-oil substrate: (a) optical microscope view; (b) scanning electron microscope view; micrographs taken by Lazarov et al. [37].

The mechanism of two-dimensional crystallization over F-oil substrate resembles that over a solid substrate (Section 13.3). Again the ordering started when the water film thickness becomes about the particle diameter, which was 1.7 μm for the used latex spheres [37]. A difference with the case of solid substrate is that as a first step small groups of particles are formed in the aqueous film. Next one observes that these groups (2D aggregates) attract each other, come closer and merge into larger ordered aggregates. The interfacial deformations around each aggregate are visible due to the formation of interference fringes in the surrounding aqueous layer of uneven thickness. Consequently, one can be sure that the observed attraction and coalescence of particle aggregates is due to the action of the lateral immersion forces (Chapter 7). At the first stages of the ordering process a "2D foam" (cf. Figs. 13.3b and 13.9) is formed. During the later stages one observes the formation of a ring-shaped homogeneous particle monolayer, which grows owing to the evaporation-driven convective supply of particles (Fig. 13.18a).

After the evaporation of the water from the F-oil surface, the oil itself starts to evaporate. The formed particle structure gradually approaches the glass plate at the bottom of the cell. After the evaporation of the oil the particle array is transferred to the solid substrate (Fig. 13.18b). In order to prepare samples for electron microscopy a specimen grid was put at the bottom of the cell before loading it with F-oil and particle suspension. After drying, the formed

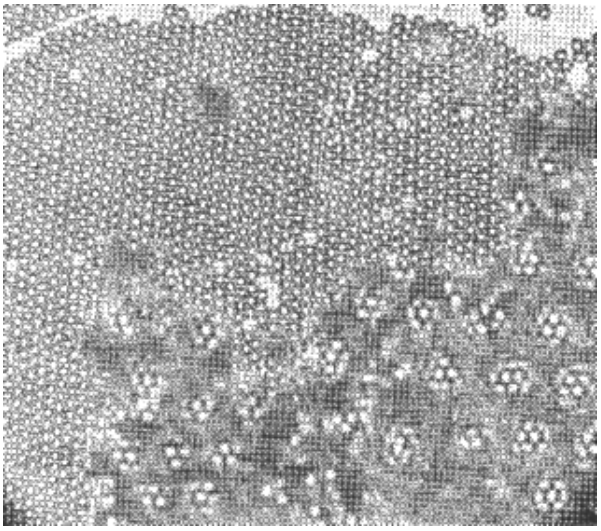

Fig. 13.20. Photograph from Ref. [37] of two overlapping ordered monolayers from latex spheres; the apparent "superlattice" (down right) is a result of the moiré optic effect.

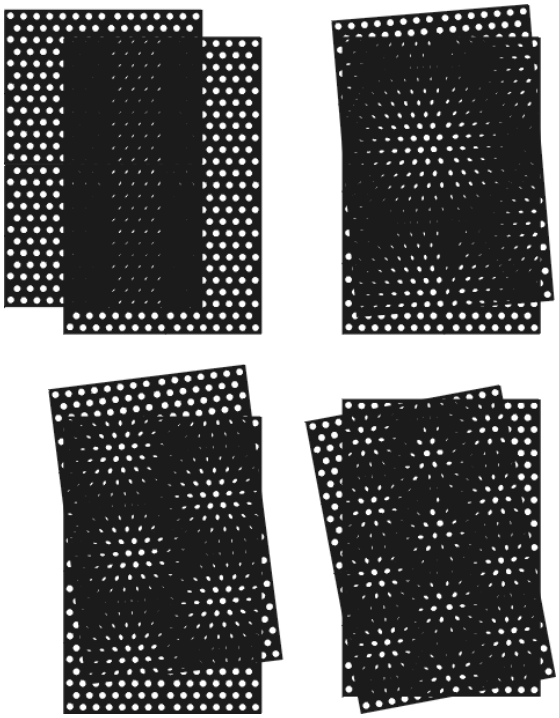

Fig. 13.21. Illustration of the moiré optic effect due to the relative rotation of two identical lattices; the dependence of the "superlattice" constant on the magnitude of rotation can be seen [37].

structures were directly deposited on the specimen grid and were studied by electron microscopy. Fig. 13.19 shows large well ordered domains of latex particles formed on F-oil substrate.

Two additional differences between the ordering on a glass (solid) and F-oil (liquid) substrate deserve to be mentioned. As noted in Sections 13.3, in some experiments with glass substrate multilayers have been obtained with the sequence of layers: 1Δ–2❑–2Δ–3❑–3Δ–··· established by Pieranski et al. [86,87] for colloid particles confined in a narrow wedge-shaped gap between two *solid* plates. In contrast, on the F-oil substrate only hexagonally (Δ) packed multilayers, 1Δ–2Δ–3Δ–···, are formed; tetragonal (❑) zones are not observed at the boundary between two hexagonal layers. This can be attributed to the "soft" oil-water interface which can bend in the transition zone between the multilayers [37].

If the rate of water evaporation is high, the approaching ordered domains (which are almost dry) can tuck one underneath another upon collision instead of merging and rearranging [37]. Then if the axes of symmetry of the two hexagonally-packed domains are rotated with respect to each other at an angle not divisible by 60°, they form a peculiar "superlattice". The latter exhibits an interesting optical property termed the "moiré effect" [177]. One observes regions of hexagonal packing of unit-cell constant larger than that of the particle monolayer (Fig. 13.20). The relation of the "moiré effect" to the relative rotation of the axes of the two 2D lattices is illustrated in Fig. 13.21.

In conclusion, the results with F-oil substrate [37] confirm that the capillary forces and the convective particle flux are the main factors governing the 2D array formation. The quality of the array can be improved by control of the evaporation rate and the meniscus shape.

13.4.2. MERCURY AS A SUBSTRATE FOR TWO-DIMENSIONAL CRYSTALLIZATION

The processes in the mercury trough (Section 13.2) happen too fast and one can examine only the final result of the two-dimensional crystallization. To investigate its mechanism, Dimitrov et al. [38] carried out separate experiments with μm-sized latex particles and recorded the

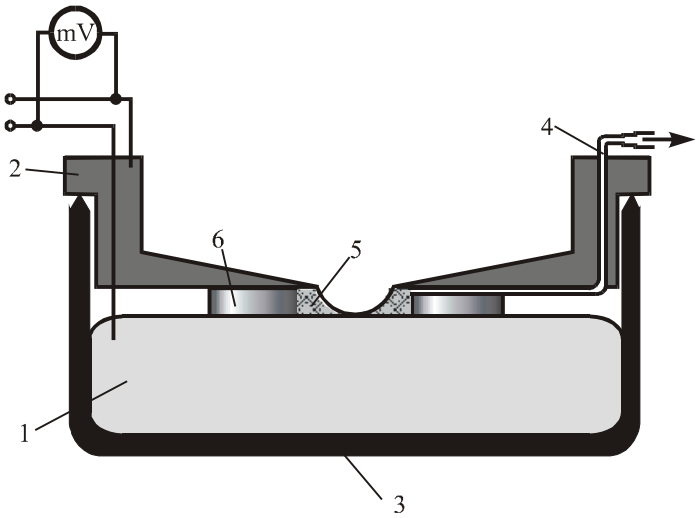

Fig. 13.22. Experimental cell used in Ref. [38] to obtain ordered 2D arrays of colloid particles on the surface of mercury: (1) mercury, (2) bronze cover, (3) container for mercury, (4) syringe needle, (5) aqueous suspension of latex particles, (6) plastic ring representing the wall of the crystallization cell.

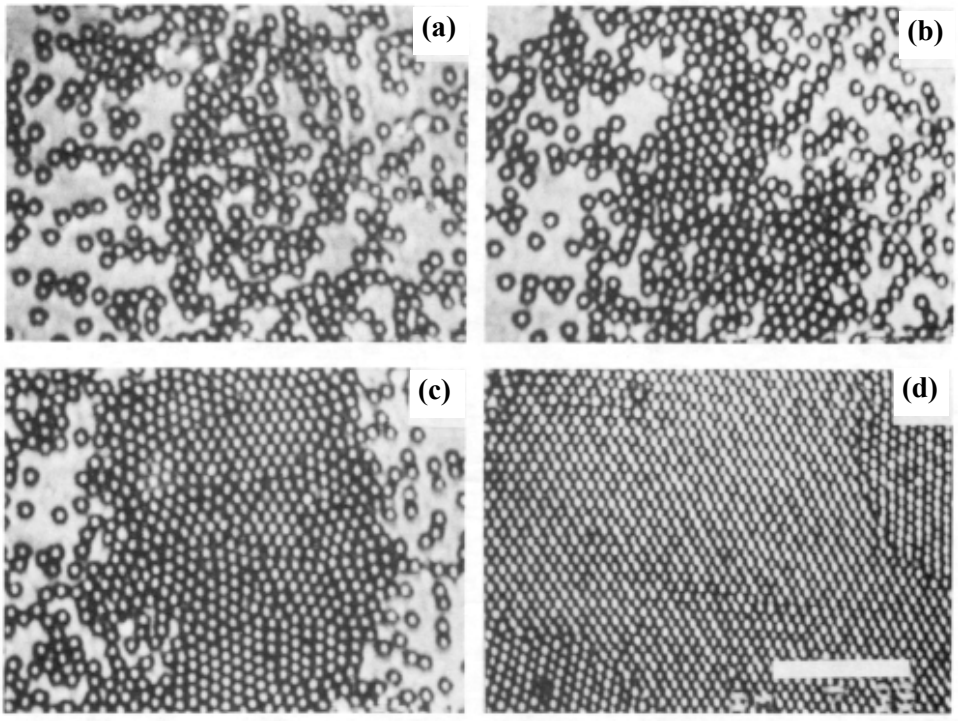

Fig. 13.23. Consecutive stages of the ordering of 1.7 μm latex spheres on the surface of mercury: (a) in the beginning ($t = 0$) the particles associate in 2D clusters; (b) at $t = 1$ min one sees an increased number of clusters; (c) at $t = 4$ min the coalescence of clusters has led to the formation of a large aggregate (nucleus), which begins to grow due to a directional influx of new particles; (d) a large ordered domain as a final result of the 2D crystallization; the length of the bar is 20 μm; micrographs taken by Dimitrov et al. [38].

dynamics of the process. For that purpose a special experimental cell was constructed (Fig. 13.22). Latex suspension layer was spread over a part of the mercury surface restricted by a plastic ring of inner diameter 1 cm. The plastic ring had thickness 1 mm and separated the bronze cover from the mercury substrate. The electric potential difference between the mercury and the bronze cover could be varied and its effect on the 2D ordering was examined. Before each experiment the mercury surface was treated with 0.01 M solution of sodium dodecyl sulfate, which ensured hydrophilization and spreading of the latex suspension droplet.

The latex particles bear a negative surface charge. When a potential equal to –200 mV, or more *negative*, is applied to the mercury, it repels the latex particles in the spread thick layer of suspension [38]. This electrostatic "buoyancy force" brings the particles on the upper (water-air) interface, where they are further observed to attract each other and to form hexagonally packed domains. At the upper interface the particles have a configuration like

that in Fig. 8.2a; hence, the attraction between them can be attributed to a counterpart of the lateral flotation force, but driven by the electrostatic upthrust rather than by the usual Archimedes force, which is due to gravity. The hexagonal particle arrays thus formed were not very stable and were destroyed by convective fluxes in the suspension layer [38].

On the other hand, if a relatively high *positive* electric potential (≥ +100 mV) is applied to the mercury, then the latex particles stick to its surface, which does not facilitate the 2D ordering.

It was found that the best conditions for 2D crystallization are provided when the potential of the mercury is low and positive, between +3 and +10 mV [38]. In this potential range uniform aqueous suspension film was formed on the mercury. The nucleation and growth of 2D particle arrays was observed in films of thickness *slightly smaller* than the particle diameter; the latter was 1.70 ± 0.05 μm for the particles in Fig. 13.23. First one sees (Fig. 13.23a) that the particles attract each other and associate into small clusters under the action of the lateral immersion force (see Chapter 7). After 1 min. the particle packing into clusters becomes denser (Fig. 13.23b); on the other hand, zones free of particles appear. After 4 min. the larger particle assemblies are observed, which are formed by coalescence of smaller clusters (Fig. 13.23c); the evaporation from the assembly triggers a slight directional particle motion towards the array. Finally, a large two-dimensional ordered array was formed; it consists of hexagonally-packed domains (Fig. 13.23d). The boundary between two neighboring domains can be removed (to form a larger domain) by a consecutive increase and decrease of the humidity of the air above the array, which causes a partial "melting" and subsequent "re-crystallization" of the 2D array; this procedure was termed "annealing" [38]. The experiments on mercury surface reported in Ref. [38] convincingly demonstrated the role of the lateral immersion forces in the process of two-dimensional aggregation and ordering of colloidal particles confined in a liquid film.

13.5. SIZE SEPARATION OF COLLOIDAL PARTICLES DURING 2D CRYSTALLIZATION

Consider an aqueous layer containing a mixture of larger and smaller particles. When the thickness of the layer decreases owing to water evaporation, the tops of the larger particles first protrude from the liquid layer, and the overlap of the menisci formed around them gives rise to a strong capillary attraction (Fig. 7.1b), which is expected to cause aggregation of

the *larger* particles. Later, with the advance of water evaporation, the tops of the *smaller* particles will also protrude from the aqueous layer and then they will also aggregate driven by the lateral immersion force. As a result, the larger and the smaller particles are expected to form *separate* aggregates. Such a size separation (segregation) of particles during 2D crystallization can serve as an indicator for the involvement of the lateral immersion force into the process of ordering.

In Ref. [33] observations of the formation of 2D array from a mixed suspension, containing particles of diameter 1.70 and 0.81 μm, are reported. It has been observed, that first the larger particles form ordered clusters, and at a later stage these clusters are encircled by ordered array of the smaller particles.

Yamaki et al. [39] carried out experiments on formation of 2D arrays of latex particles in the mercury trough, see Section 13.2.1. The average size of the particles was 55 nm and their polydispersity is characterized with a standard deviation ±3.4 nm. In the resulting arrays (see Fig. 13.24a) ordered clusters of the largest particles are surrounded by 2D array of the smaller particles; the particle size decreases with the increase of the distance from the center of the cluster. As discussed above, this effect can be attributed to the fact, that the largest particles first protrude from the thinning liquid layer and are grouped together by the lateral immersion force to form a 2D aggregate. The evaporation from this aggregate brings about a convective influx of water. The flow carries along suspended particles; only those of them, whose tops protrude from the liquid layer, can be captured by the aggregate owing to the capillary attraction. Since the thickness of the aqueous layer decreases with time (due to the evaporation), smaller and smaller particles are able to join the aggregate; the latter explains the decrease of the particle size with the increase of the distance from the center of the cluster. This phenomenon could be further developed into a method for size-fractionating of colloidal particles, including proteins and viruses [39].

Yamaki et al. [39] performed experiments in the mercury trough also with mixtures of larger and smaller particles. Examples for the observed size separation are shown in Figs. 13.24 b-d. As a rule, the larger particles are collected in the center of the aggregate and are surrounded by an ordered array of the smaller particles. In Fig. 13.24b the larger, 144 nm in diameter, latex

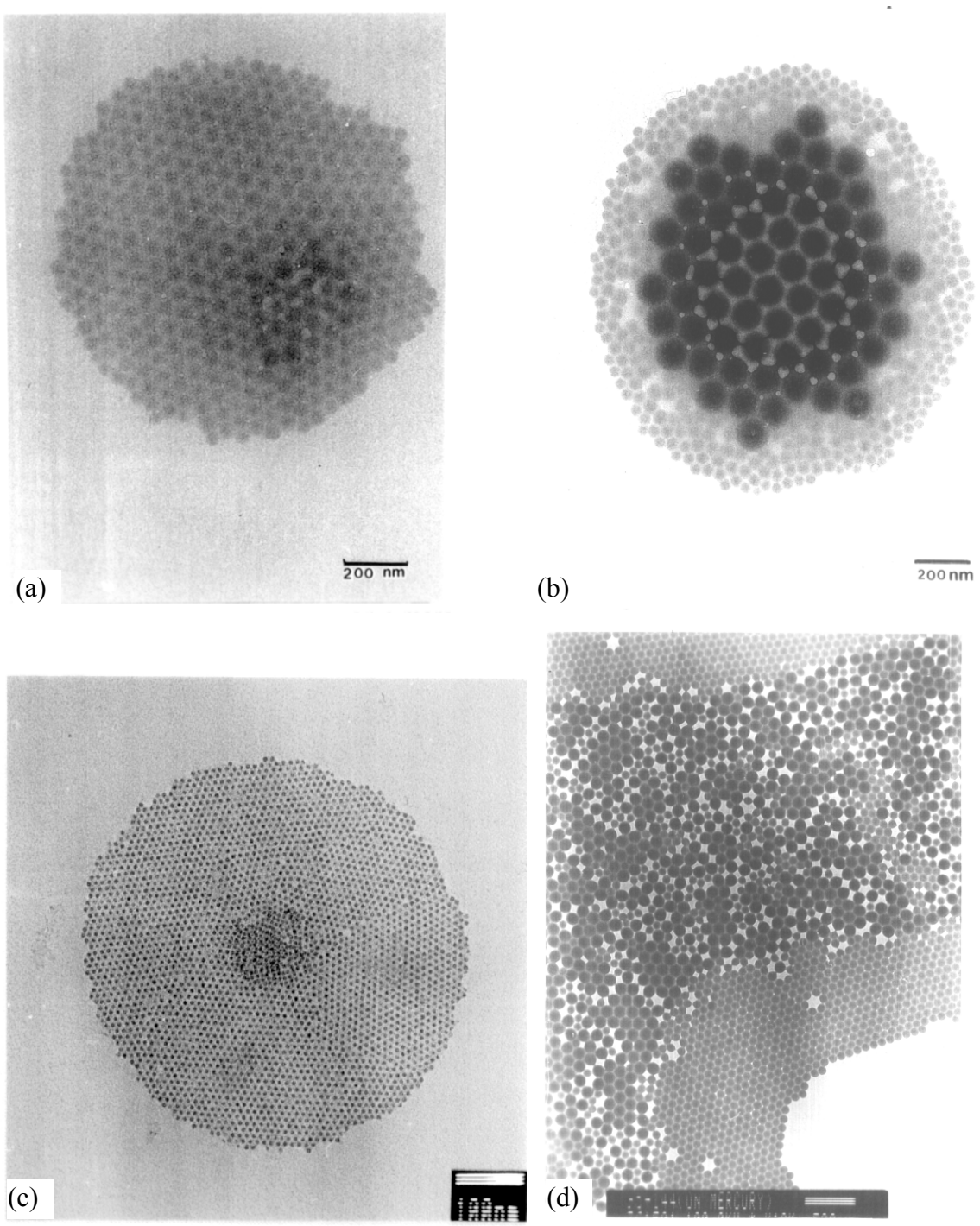

Fig. 13.24. Effect of size separation during 2D crystallization: transmission electron microscope images taken by Yamaki et al. [39] from samples of 2D arrays formed in a mercury trough: (a) from polydisperse latex spheres of diameter 55 ± 3.4 nm; (b) from a homogenized suspension mixture containing latex particles 55 ± 3.4 nm and 144 ± 2.0 nm in diameter; (c) from a mixture containing the protein ferritin and polio virus of diameters 12 nm and 30 nm, respectively; (d) from a suspension mixture containing latex particles 95 ± 2.0 and 144 ± 2.0 nm in diameter.

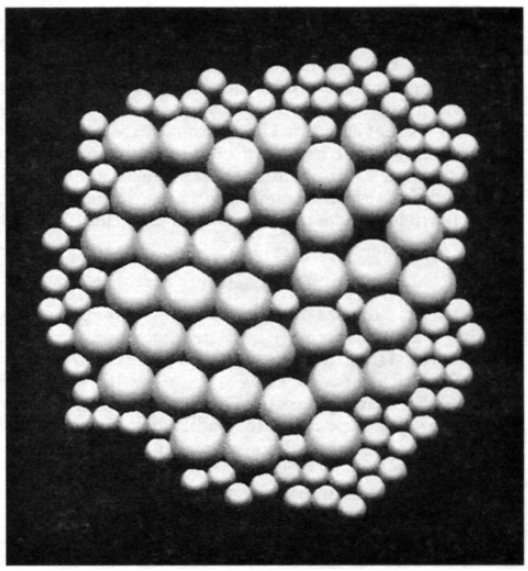

Fig. 13.25. A result from the computer simulation of 2D size separation in a mixture of larger and smaller particles (diameter ratio 2:1) in the presence of evaporation and capillary immersion force [39].

spheres (in the center) are separated from the smaller latex particles of diameter 55 nm. Similar result was obtained with a mixture of latex particles of diameter 22 nm and ferritin (protein) molecules of diameter 12 nm [39]. In Fig. 13.24c the polio viruses of diameter 30 nm are grouped in a small cluster in the center, surrounded by the separated ferritin molecules. The separation of the larger from the smaller particles is not good when there is a relatively strong attraction between the particles of the two different species. The theory of the double-layer interactions [95] predicts that colloid particles of *different* surface potential could experience electrostatic attraction at short distances, even when the surface potentials have the same sign. An effect of this type was observed with a mixture of polystyrene latex particles of diameters 144 and 95 nm [39], see Fig. 13.24d.

To obtain a better understanding of the observed size separation, computer simulations were also carried out by means of the Monte Carlo method [39]. The behavior of the particles in a mixture of 37 large and 84 small particles was simulated in the presence of lateral capillary force and convective flow. The computer simulations reproduced a size separation (Fig. 13.25), which is very similar to the experimental results.

It is interesting to note that almost simultaneously with the work by Yamaki et al. [39] another work reporting a similar phenomenon appeared. Ohara et al [178] studied the formation of 2D crystals (opals) from suspensions of polydisperse nm-sized gold particles in hexane. The resulting structures were detected by means of transmission electron microscopy (TEM). In some of the experiments a drop of such suspension was evaporated directly on an amorphous carbon-coated TEM grid. In other experiment a layer of the gold-in-hexane suspension was evaporated over water in a 10 cm diameter Petri dish and a sample for TEM was taken after the evaporation of the hexane. In both cases it was found that hexagonally-packed domains of the largest particles (5-6 nm diameter) were formed at the center, which were surrounded in radial direction by successively smaller particles.

Ohara et al. [178] hypothesized that the size separation of the particles is due to the size dependence of the van der Waals attraction between the gold particles. Computer simulations of the process of ordering was carried out by means of the Monte Carlo method in conjunction with the Hamaker formula for the van der Waals interaction between two spherical particles of different radii. The computer simulation reproduced a size separation, which is very similar to the experimental results [178].

Then a question arises: which is the cause for the particle size separation – the van der Waals surface force or the lateral capillary force? For the system studied by Ohara et al. [178] perhaps both of them are simultaneously operative and the size segregation happens under their combined action. On the other hand, the proteins, viruses and latex particles have a very low Hamaker constant across water: $A_H = 5\text{-}8 \times 10^{-21}$ J for two protein molecules across water [179], whereas $A_H = 3.1 \times 10^{-19}$ J for two gold particles across dodecane [178]. For that reason, it is unlikely the van der Waals forces to play an essential role in the ordering and size separation observed by Yamaki et al. [39]. Moreover, for particles of radius greater than 10 nm the energy of the capillary immersion interaction becomes larger than 100 kT (see Fig. 8.3), which is certainly much greater than the energy of the van der Waals attraction between such particles, except might be at close contact.

The effect of size separation under the action of the lateral immersion force and convective flux was confirmed both experimentally (polydisperse latex particles of average size 80 and

220 nm) and by computer simulations by Rakers et al. [180]. The 2D arrays were formed on a silicon substrate, whose temperature could be varied. At lower temperatures (2°C) a more pronounced effect of ordering and size segregation was observed as compared with the result at higher temperature (20°C). The temperature affects the 2D crystallization through the rate of evaporation. At higher temperature the evaporation is stronger and the growth of the ordered aggregates is dominated by the convective flux, rather than by the lateral capillary force. As a result, the size selection carried out by the capillary force is suppressed. In contrast, at low evaporation rates (low temperatures) the uptake of particles by the aggregates is dominated by the capillary force, which brings about a size segregation of the particles.

13.6. METHODS FOR OBTAINING LARGE 2D-CRYSTALLINE COATINGS

13.6.1. WITHDRAWAL OF A PLATE FROM SUSPENSION

For examination of 2D arrays of sub-μm particles and protein macromolecules by electron microscopy relatively small (microscopic) samples are sufficient. On the other hand, the usage of 2D arrays in industrial applications may demand the formation of larger ordered areas (1 cm^2 and larger) [40,41]. As discussed in Section 13.3, the two-dimensional crystallization in a cylindrical cell (Figs. 13.4 and 13.14) gives ordered domains of area not larger than 1 mm^2 due to the appearance of instabilities in the crystal growth (consecutive formation of monolayers and multilayers). In principle, this problem could be overcome by adjustment of the rate of receding of the capillary meniscus in such a way, that a particle monolayer to be formed. In other words, the velocity of the contact line array/meniscus is to be determined by Eq. (13.9) with $h = 2R_p$,

$$v_c = \frac{\beta \; j_e V_w \phi \; b}{2R_p \phi_a (1-\phi)} \quad , \qquad \text{(for monolayer)} \qquad (13.16)$$

where R_p is the particle radius. A possible way to realize receding of the meniscus, with a velocity v_c given by Eq. (13.16), is to withdraw a hydrophilic plate from a suspension with a constant speed. This was realized by Dimitrov and Nagayama [40] as described below, and cm-sized 2D arrays of colloidal particles were obtained on hydrophilic glass plates.

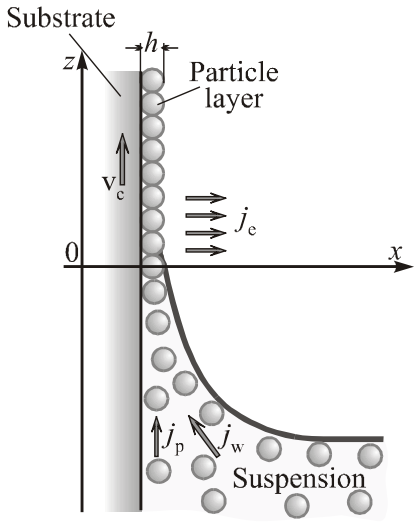

Fig. 13.26. The withdrawal of a plate from a suspension carries along a liquid film containing particles; the evaporation of the solvent (water) from that film gives rise to a convective influx of water j_w and particles j_p; the latter stick to the periphery of the growing array arrested by the capillary immersion force.

In the beginning of each experiment the plate (in vertical position) is immersed partially into a suspension of monodisperse latex spheres. The water rises along the hydrophilic plate to form a very small (practically zero) contact angle. The wedge-shaped meniscus just below the contact line contains latex particles. Because of water evaporation from the suspension, the level of the liquid slowly decreases, which results in a deposition of latex particles on the vertical glass substrate in the zone of the receding contact line. In fact, this is a known phenomenon: always when water contacts with wettable surfaces and evaporates, the substances dissolved in the water accumulate in the wetting film in the vicinity of the three-phase contact line [40,59].

An initial deposit of latex particles is thus obtained; then a stepper motor is switched on and the glass plate is pulled up out of the suspension with an appropriate rate in the range from 0.1 to 30 μm/s. The particle array deposited on the plate is observed by microscope and the rate of plate withdrawal, v_c, is adjusted to obtain a monolayer in a stationary regime of continuous 2D array growth (Fig. 13.26). Monodisperse suspensions of particle radii ranging from 79 nm up to 2.1 μm have been used at fixed particle volume fraction: $\phi = 0.01$. It has been established experimentally [40] that $v_c \propto 1/R_p$, exactly as predicted by Eq. (13.16). If v_c is decreased two times by the stepper motor, one observes formation of a particle bilayer.

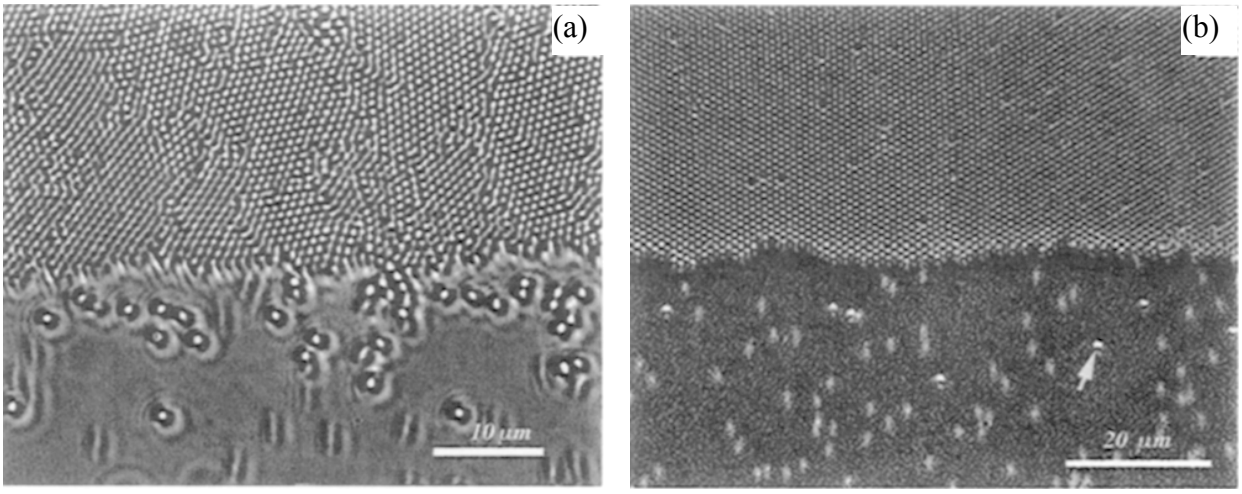

Fig. 13.27. Photographs from Ref. [40] of the region around the border of growing 2D array on a vertical plate, which is being pulled up from an aqueous suspension, which contains particles of diameter (a) 814 nm and (b) 953 nm. The particles in the liquid film below the array are dragged upwards by the evaporation driven water flow (Fig. 13.26); particles moving during the exposition period look fuzzy; the arrow in (b) indicates one of the larger particles immobilized in the thicker water film below the boundary of the array.

As already discussed in Section 13.3, the growth of particle 2D array in the experimental cells depicted in Figs. 13.4 and 13.14 happens through an evaporation-driven convective flow of water, which brings along suspended particles toward the boundary of the 2D array; once reaching that boundary the newcomer-particles are captured by the lateral capillary force and firmly attached to the growing array. Neither the convective flow, nor the capillary interaction is dependent on the gravitational force, so one could expect that the mechanism of growth is not dependent on the orientation of the plate: horizontal (Figs. 13.4, 13.14 and 13.17) or vertical (Fig. 13.26).

By means of optical microscope it was observed that in stationary regime of the plate withdrawal the width of the wet zone is $b \approx 2$ mm [40]. Similar value of b was obtained from Eq. (13.16) using experimentally measured values of v_c and j_e. The microscopic observations showed also the existence of directional motion of particles, dragged by the water flow toward the boundary of the growing array, see Fig. 13.27. Some bigger particles are immobilized before reaching the array and subsequently they cause defects in the 2D crystal, cf. Fig. 13.27 and 13.6b. All these similarities between the 2D array formation on a horizontal and vertical substrate imply that the underlying physical mechanism of growth is essentially the same. The

advantage of the technique with vertical plate is that the rate of withdrawal can be relatively easily controlled to obtain large ordered particle monolayers in a continuous regime of production [40].

The formed dried ordered monolayers exhibit uniform coloring due to interference of light, cf. Table 13.2. Moreover, the 2D arrays from particles, whose diameter is greater than the wavelength of the visible light, exhibit brilliant (opalescent) diffraction colors, which depend on the particle size and the orientation of the 2D crystal domains. The brilliant coloring can be enhanced by coating the particulate monolayers with silver or gold (up to 10 nm thick); the coating stabilizes mechanically the arrays, which are fragile before the metal coating. The usage of these ordered arrays as diffraction gratings is discussed in Ref. [40,41].

13.6.2. DEPOSITION OF ORDERED COATINGS WITH A "BRUSH"

As discussed above, larger domains of ordered 2D arrays can be obtained if the speed of meniscus receding, v_c, is appropriately related to the evaporation flux j_e and the width of the wet array, b, see Eq. (13.16). An experimental method, which allows a control of v_c and j_e was developed in Ref. [42] and successfully applied to obtain large 2D crystals of the protein holoferritin. The basic part of the experimental setup is shown in Fig. 13.28. The substrate is a silicon wafer (20 × 20 × 1 mm), which is fixed to a movable horizontal stage. A vertical platinum plate (20 × 20 × 2 mm) plays the role of a "brush". In the experiments 10 microliters protein solution is introduced at the corner between the horizontal silicon wafer and the vertical Pt-plate. Then by means of a motor the stage with the silicon wafer begins to move horizontally with a constant velocity of 2 μm/s. After the receding meniscus, which is attached to the vertical Pt-plate, a thin wetting film is deposited on the silicone substrate. Large and ordered two-dimensional arrays of protein are formed in the drying film: this was established by scanning electron microscope [42].

It was established that better two-dimensional arrays of holoferritin are formed when the humidity of the atmosphere above the deposited film is higher and the rate of evaporation is lower [42]. Moreover, it was found experimentally, that good hexagonal ordering is obtained when the pH is sufficiently higher than the isoelectric point of the holoferritin (at pH = 4.8),

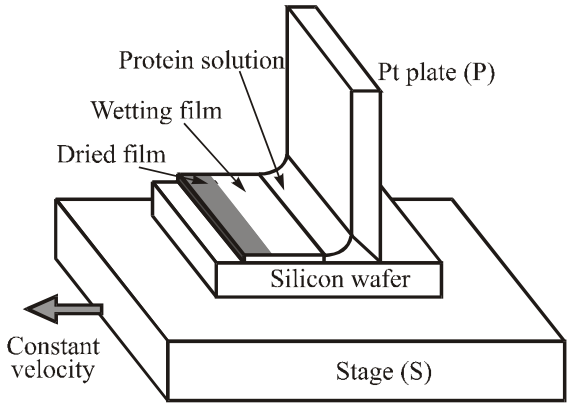

Fig. 13.28. Deposition of a film from protein or particulate suspension over a moving horizontal substrate with the help of an immobile vertical plate: sketch of the experimental setup used in Ref. [42].

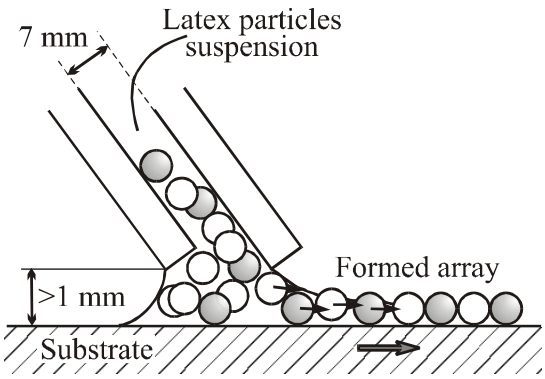

Fig. 13.29. Deposition of a film from latex-particle suspension over a moving horizontal substrate with continuous supply of suspension through a channel of width 7 mm between two parallel plates: experimental setup used in Ref. [43].

and respectively, the protein is negatively charged. The latter effect could be attributed to the electrostatic repulsion between the negatively charged protein and the silicon substrate, which prevents irreversible protein-to-silicon attachment and promotes the arrangement of the molecules into a regular hexagonal lattice.

A method, which allows a continuous supply and deposition of the suspension was developed in by Matsushita et al. [43]. The suspension was supplied by means of an extruder (Fig. 13.29), which was constructed from two parallel glass plates (25 × 25 mm); the width of the gap between them was 0.7 mm. After injection of suspension in the gap of the extruder, the glass substrate was translated horizontally with a constant speed, which was fixed at 5 μm/s in order to form a monolayer of latex particles. In the beginning an wetting film from the suspension is deposited. During the drying of this film the latex particles are ordered into a hexagonal lattice by the attractive lateral capillary forces [43]. In the specific experiment a mixture of fluorescent and non-fluorescent latex particles of equal diameters, 1.00 ± 0.05 μm was used. The quality of the obtained 2D ordered arrays was found to increase with the increase of the particle charge, which can be attributed to the enhanced particle-substrate and particle-particle repulsion. In a subsequent experimental study Matsushita et al. [181] applied their technique to create large 2D arrays of ordered SiO_2 particles, which were further used as

a matrix for fabrication of mesoporous structured TiO_2 films exhibiting photocatalytic activity.

13.7. 2D CRYSTALLIZATION OF PARTICLES IN FREE FOAM FILMS

13.7.1. ARRAYS FROM MICROMETER-SIZED PARTICLES IN FOAM FILMS

In the previous sections of this chapter we considered two-dimensional structuring of particles in wetting films formed on substrates. Particle structuring can be realized also in free liquid films formed between two gas phases (foam films). Experimental studies on particle structuring in such films revealed the features and advantages of this approach to the obtaining of 2D arrays [44-47].

In Ref. [47] the foam films were formed from a suspension of latex particles having diameter 7 μm and bearing a negative surface potential (about −70 mV). The processes of particle agglomeration and ordering were observed by optical microscopy. To form the films, the liquid was gradually ejected from a cylindrical capillary in the experimental cell invented by Scheludko & Exerowa [182,183], see Fig. 13.30. During the measurements the experimental cell was kept in a closed environment saturated with water vapor, which prevented the evaporation from the film surfaces. After the formation of a liquid film, its thickness progressively decreases because of a continuous outflow of water from the film towards the encircling Plateau border. It was established that the nature of the dissolved surface-active agent, used to stabilize the thin film, has a crucial impact on the observed phenomena [47].

In some experiments the films were stabilized by the addition of 0.016 M sodium dodecyl sulfate (SDS), which is an *anionic surfactant*. Experimentally it was observed that although the thick films contained latex particles, in the course of film thinning all particles were pushed out of the film area [47], see Fig. 13.31a. Therefore, particle ordering was not detected in the foam film. The main reason for this negative result is the convective outflow of water from the film, which is not essentially resisted by the adsorption monolayers from SDS at the film surfaces insofar as SDS exhibits a low surface viscosity upon adsorption [184]. Moreover, both the latex particles and the film surfaces bear a negative surface charge, and consequently, repel each-other.

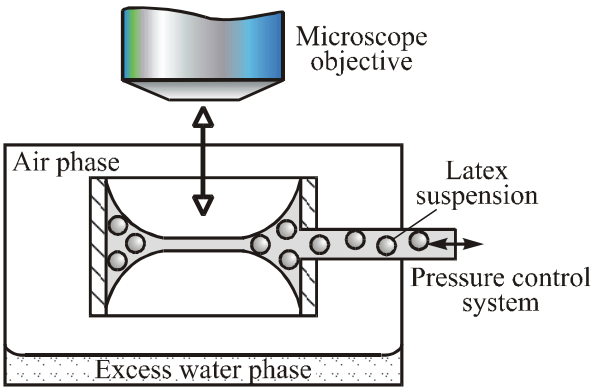

Fig. 13.30. Sketch of the experimental setup used in Ref. [47] to produce ordered 2D arrays from negatively charged spherical colloid particles in a freely suspended foam film.

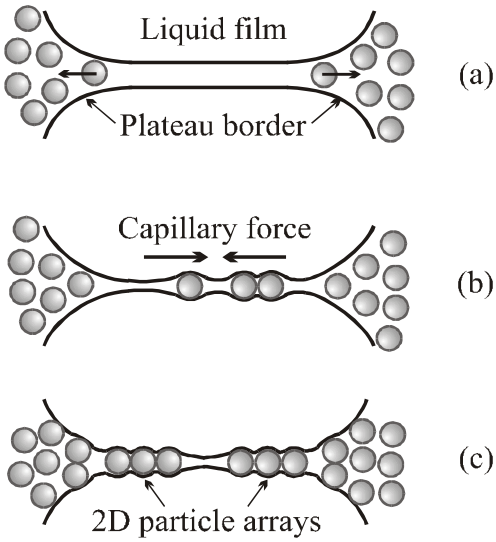

Fig. 13.31. Schematic description of the experimental results obtained in Ref. [47]: (a) with anionic surfactant (SDS) all particles are expelled from the film; (b) with protein (BSA) some particles are entrapped in the film and experience long-ranged attraction; (c) with cationic surfactant (DTAB, HTAB) large and well-ordered arrays of particles can be formed.

In another cycle of experiments, to increase the surface viscosity the films were stabilized with the addition of 0.1 wt % *protein*, bovine serum albumin (BSA), instead of SDS [47]. In this case it was possible to entrap latex particles within the foam film. The captured particles tended to form small 2D aggregates; the latter were observed to attract each other from distances, which could reach up to 100 μm (Fig. 13.31b). This attraction can be attributed to the lateral immersion force, see Fig. 7.1f. At higher particle concentration the formation of array having "2D-foam" structure was observed. On many occasions the entrapped particles caused rupture of the otherwise stable film [47].

Best 2D arrays of negatively charged latex spheres were formed in films stabilized by a *cationic surfactant*, like dodecyl-trimethyl-ammonium bromide (DTAB) and hexadecyl-trimethyl-ammonium bromide (HTAB). In this case latex particles adhered to the surfactant

adsorption monolayers at the air–water surfaces. As a result, the particle mobility was much decreased and interfacial deformations appeared when the particles bridged the two film surfaces; the latter caused a strong interparticle capillary attraction (Fig. 7.1f). At a higher surfactant concentration (0.03 M DTAB) bulk aggregation of the latex particles was observed, which was undesirable. Best hexagonal 2D arrays were observed for an intermediate surfactant concentration, viz. 0.006 M DTAB. The ordering induced by the lateral capillary force started as a ring-shaped zone at the periphery of the circular film (Fig. 13.31c). By a series of consecutive increasing and decreasing of the pressure in the Plateau border (shrinking and expansion of the contact line) it was possible to rearrange the ring-shaped array into a large compact 2D array with excellent hexagonal packing, which covered the whole film area [47].

Part of the difficulties encountered in Ref. [47] are due to the fact that the cell with the foam film has been kept in a closed environment with saturated aqueous vapor, which has prevented the evaporation. Therefore, the predominant convective flux was directed *outwards* and pushed the particles out of the film; the only factor promoting the 2D aggregation in this case was the lateral immersion force.

On the contrary, if evaporation from the foam film is present, it causes a radial water *influx*, from the Plateau border towards the center of the film. As discussed in section 13.3.1 the influx brings new particles within the film and in combination with the capillary force leads to a 2D crystal-growth. The latter mechanism (combined convective flux and capillary force) has been employed by Denkov et al. [44-46] to obtain two-dimensional crystals of sub-μm particles in free foam films; see the next section.

13.7.2. ARRAYS FROM SUB-MICROMETER PARTICLES STUDIED BY ELECTRON CRYOMICROSCOPY

2D arrays of sub-μm particles cannot be detected by usual optical microscopy. For that reason a special experimental technique was developed in Refs. [44,45] to accomplish observation of structures in free foam films by means of electron microscopy. At a given stage of the experimental procedure the foam film was frozen by a quick immersion into a cooling liquid, which was 1:1 mixture of ethane and propane at –190°C. Such a sudden cooling led to a vitrification of the aqueous films, that is formation of amorphous ice. (The appearance of any

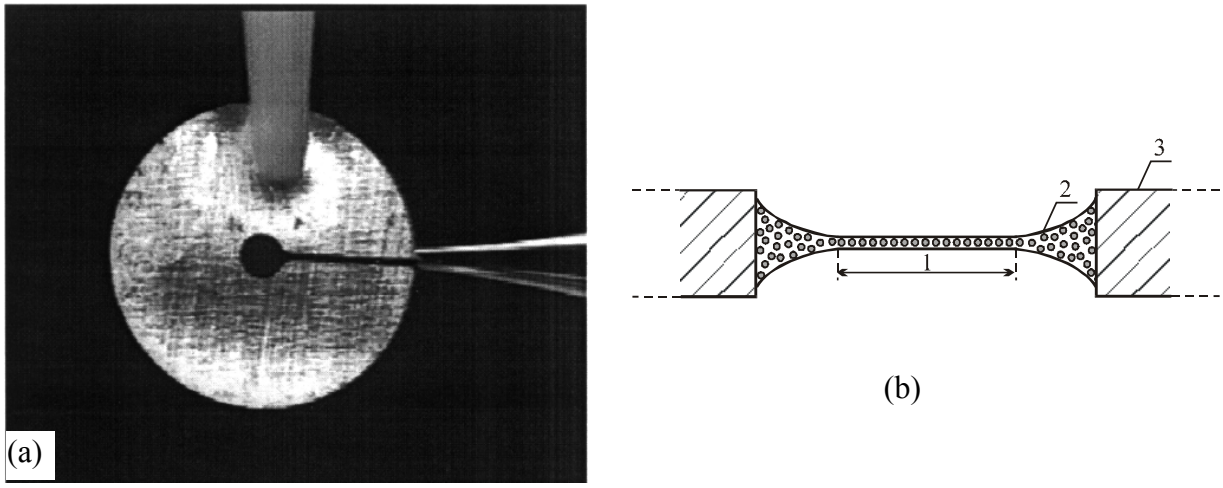

Fig. 13.32. (a) Photograph of the disk-shaped holder made of copper, which was used by Denkov et al. [44-46] to produce and cryo-vitrify 2D arrays in free foam films. The foam film is created in the central hole (the dark circle in the center of the holder), which is first loaded with a droplet of particle suspension; a glass capillary attached to the holder (on the right) is used to suck out liquid from the loaded droplet through a narrow slit. (b) Thus a free foam film (1) is formed, which is encircled by a meniscus border (2) attached to the inner edge of the holder (3).

ice crystals would damage the structures formed within the foam film.) In these experiments a free foam film of relatively large diameter (≈ 100 μm) was created in the central hole of a disk-shaped copper holder (Fig. 13.32a); the latter was 60 μm thick and had an outer diameter 3 mm. The central hole was connected by a narrow channel with the periphery of the holder. During the film formation and the subsequent thinning the tip of a glass capillary was attached to the outer end of the channel. The capillary was connected to a microsyringe, which supplied the investigated suspension for creating a film in the hole (Fig. 13.32b), and allowed for the precise control of the film diameter. The thickness of the foam film was determined by means of an optical interferometric method with accuracy of about ±1 nm [44,45].

The formation of 2D arrays in free foam films is based on the same mechanism as the 2D crystallization in wetting films (Section 13.3.1), i.e. on the combined action of capillary forces and evaporation-driven convective flux, see Fig. 13.33. Initially, a relatively small film (diameter ≈ 30 μm) is created and then the contact line encircling the film is gradually expanded up to diameter 100–150 μm. In this way, an ordered monolayer is formed within the film if the particle concentration in the bulk suspension (about 10 vol%), the rate of film expansion (5–10 μm/s), and the evaporation rate are appropriately chosen. If the optimal

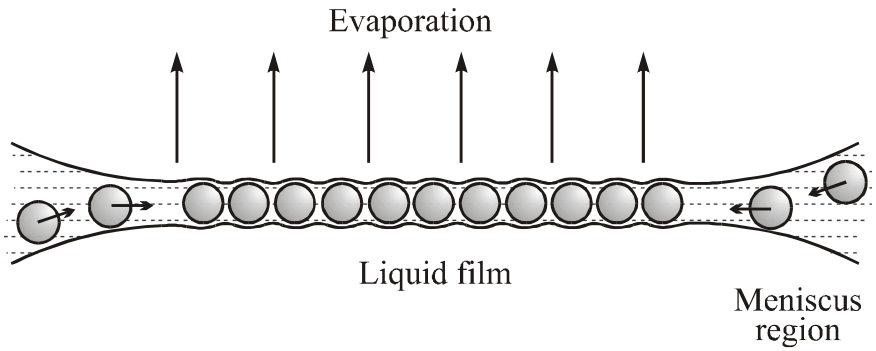

Fig. 13.33. Sketch of the process of particle ordering in an evaporating free foam film. A flux of particles directed from the meniscus region toward the film appears as a result of the water evaporation from the film region. The particles-newcomers are arrested at the periphery of the growing array by the attractive capillary immersion force.

regime is violated, the quality of the formed array worsens. For example, at lower particle concentration and/or at a faster expansion of the contact line one obtains films deprived of particles. On the other hand, a higher particle concentration and enhanced evaporation result in thick films containing bilayers and multilayers [45].

After the gradual expansion of the contact line and the (hoped for) production of 2D array within the film, the glass capillary is detached from the holder with the film (Fig. 13.32a) and the latter is plunged for vitrification into the 1:1 liquid mixture of ethane and propane cooled by liquid nitrogen. Then the vitrified film is transferred into the electron microscope by means of a cryo-transfer holder. The vitrified foam films are rather fragile and any mechanical disturbance easily brakes them. For that reason the safe transfer of the frozen films into the electronic microscope is the most delicate step in these experiments. With this procedure 30% of the films thicker than 40 nm have been safely transferred into the microscope. In several experiments even films of thickness 30 nm have been transferred intact. It is expected that by means of appropriate automation the observation of films as thin as 20 nm will become attainable [44,45].

Using this method ordered monolayer of polystyrene latex spheres (66 and 144 nm in diameter) were obtained [44,45]. It is curious to note, that a vitrified aqueous film, containing a monolayer of latex particles, is much more fragile than a film of the same thickness but without particles. As a rule, the latex-containing frozen films brake along some of the

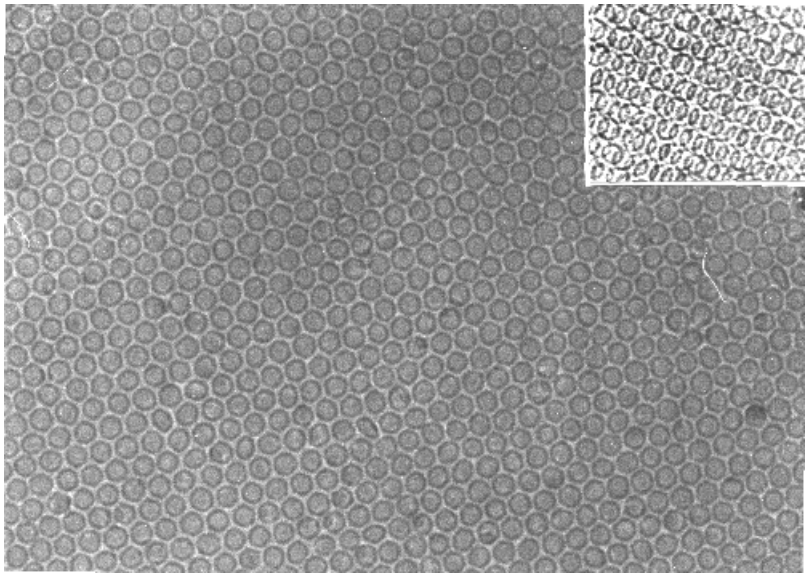

Fig. 13.34. Ordered monolayer of bacteriorhodopsin vesicles formed within a free liquid film of thickness 59 nm; the determined average radius of the vesicles is R_0 = 18.5 nm with a standard deviation $\Delta R = \pm$ 1.1 nm, which is due to their polydispersity; the inset shows an ordered bilayer of vesicles; micrographs taken by Denkov et. al. [45] with the help of cryo-vitrification of the foam film and electron microscopy.

axes of the hexagonal array [45]. In other experiments [44-46], vesicles (diameter ≈ 39 nm) made of the membrane protein bacteriorhodopsin and lipids were ordered into large hexagonal monolayers or bilayers, see Fig. 13.34. The structure of these fine vesicles cannot be investigated by the negative staining method because they are easily deformed and even totally destroyed by the staining agent. For that reason the electron cryomicroscopy is an appropriate method to investigate such soft and delicate particles. By controlling the rate of evaporation from the film (Fig. 13.33) large ordered domains (thousands of particles) have been formed. The averaged value of the vesicle radius from many studied samples was R_0 = 18.5 nm with a standard deviation ΔR = 1.1 nm, which represents a polydispersity of 6 %.

Analyzing the electronic micrographs, such as Fig. 13.34, it is possible to determine the bending elasticity of the vesicle membrane [46]. Indeed, these vesicles are formed spontaneously: purple membrane is subjected to the action of surfactant (octylthioglucoside), which dissolves selectively lipids from one of the two membrane constituent lipid monolayers. This gives rise to a spontaneous curvature, whose radius can be identified with

the experimental mean value R_0. Then with the help of the fluctuation theory [185] one can derive a Gaussian size distribution of the vesicles [46]:

$$C(R) = C(R_0)\exp\left[-\frac{2\pi k_t}{kT}\left(\frac{R-R_0}{R_0}\right)^2\right], \qquad (\Delta R)^2 = \frac{kT}{4\pi k_t}R_0^2 \qquad (13.17)$$

where $C(R)$ is the concentration of vesicles of radius R and k_t is the total bending elastic modulus of the membrane. Then from the experimental value of the standard deviation ΔR, determined from Fig. 13.34, Denkov et al. [46] calculated $k_t = 0.87 \times 10^{-19}$ J. (For lipid bilayers k_t is usually of the order of 10^{-19} J, see e.g. Eq. (10.52) above.)

In conclusion, free foam films combined with the described vitrification cryo-technique can serve as a method for obtaining and investigation of 2D arrays from colloidal particles. This method ensures the excellent structure preservation of delicate hydrated molecular complexes and fine vesicles.

13.8. APPLICATION OF 2D ARRAYS FROM COLLOID PARTICLES AND PROTEINS

13.8.1. APPLICATION OF COLLOID 2D ARRAYS IN OPTICS AND OPTOELECTRONICS

The first studies of colloid crystals from latex particles revealed that they exhibit color *diffraction* patterns and it was suggested these crystalline arrays to be used as spectroscopic diffraction gratings [18]; see Ref. [186] about more recent results. It should be noted that the precious opals, mined mostly in Hungary and South Australia, show brilliant colors due to the same diffraction effect. The colors in the opals are caused by a regular array of silica particles, whose diameter and spacing determine the color range of an opal. Similar hexagonal arrays of particles determine the coloring of the wings of the *Morpho* butterfly [187, 40, 41].

Moreover, ordered multilayers from transparent spherical particles exhibit *interference* colors [36], see Table 13.2. It is interesting to note that this effect has been utilized in the eye of the night moth, which is covered with a 2D array of 150 nm particles. This ordered monolayer allows the moth eye to remove light reflections making the most of the light available in the dark night. This example suggests application of coatings from particulate arrays for production of antireflection optical surfaces and elements.

Hayashi et al. [188] demonstrated that the separate particles from a monolayer of μm-sized latex spheres produce imaging of an object in a fashion similar to that of a compound eye. It is interesting that these small particles are fulfilling finely a lens function in a microfield beyond the range of the unassisted eye [188].

The usefulness of ordered arrays from latex spheres as a standard for determining the magnification and shadow-casting angle in electron microscopy was reported by Backus and Williams [17] and discussed by Gerould [19]. Such standards can be also serviceable for the test of novel observation schemes, like that reported in Ref. [189], aimed at improvement of the contrast and the point resolution of the electron microscopy. In addition, colloidal nanostructures can be used as test samples for optical nearfield microscopy [190,191].

A promising application of ordered arrays from semiconductor nanocrystallites is to utilize them as a photo- and electro-luminescent material [192-196]. This application stems from the fact that some fundamental properties of the solids are characterized by length scales on the order of 1 to 20 nm; if a crystal has at least one of its dimensions smaller than the length scale of the same property, then that property is "confined" and becomes dependent on the size and shape of what is now called a "quantum crystal" [196]. As a result, such quantum crystals may exhibit fundamentally new properties. For example, sufficiently small (≈ 2 nm) silicon crystallites can become a very efficient photo- and electro-luminescent material, despite the fact that the macroscopic Si crystals are not a useful optoelectronic light source [196]. For device-oriented applications such nanocrystallites have to be assembled into superlattice structures termed also quantum dot lattices [193, 197, 198].

13.8.2. NANO-LITHOGRAPHY, MICROCONTACT PRINTING, NANOSTRUCTURED SURFACES

As already mentioned, technological applications demand fabrication of small surface structures approaching dimensions of a few nanometers. The widely used photo-lithographic techniques have some limitations [199, 200]. A new, complementary technique has been proposed, which employs 2D arrays of sub-μm colloid spheres as masks for etching or vacuum deposition. Such masks are suitable in applications, in which a periodic arrangement of the structures is required. The latter technique has been termed "natural lithography" [55]

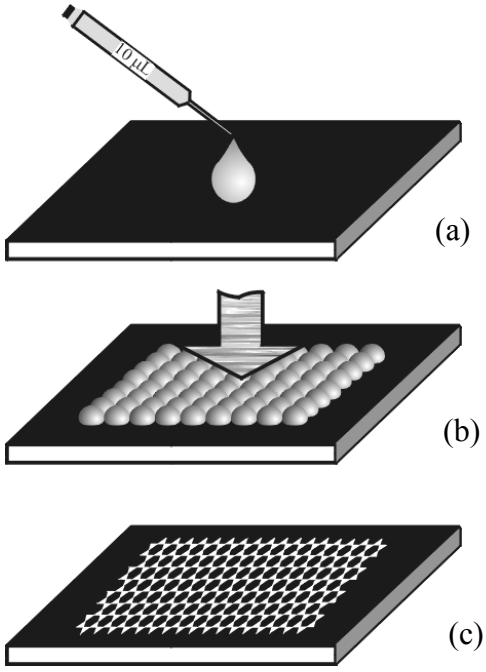

Fig. 13.35. Schematic description of the colloid-monolayer lithography (after Burmeister et al., Ref. 199): (a) droplet of suspension is spread and dried on a given substrate to obtain an ordered particle monolayer; (b) metal is deposited onto the particle monolayer; (c) regularly arranged metal structures are found on the substrate after removal of the particles.

or "nanosphere lithography" [58]. Its principle is illustrated in Fig. 13.35. First an ordered 2D array of particles is formed on a substrate by evaporation of a suspension film (see Section 13.3). Then metal is deposited using the 2D array as a *deposition mask*.

For example, Fischer and Zingsheim [201] formed an array from sub-µm polystyrene spheres on a glass substrate. Then a vacuum deposition of platinum led to the formation of triangular platinum spots on the substrate, which are located in the gaps (interstices) among the hexagonally packed polystyrene spheres. The spheres were finally removed by sonification in benzene.

Likewise, Deckman and Dunsmir [55] formed a hexagonal array of 400 nm polystyrene spheres and evaporated silver to form triangular silver posts on the substrate; next, the spheres were dissolved in methylene chloride. Alternatively, these authors used a monolayer of latex particles as an *etching mask*. A hexagonal 2D array from the polystyrene spheres was assembled on a silicon wafer. Then the silicon was etched with a 500-eV ion beam produced

from CF_4 gas discharge. Finally, the polystyrene particles were removed from the apex of the silicon posts with a 500-eV oxygen ion beam. Morphology of the individual posts can be altered by changing the reactivity of the ion beam and/or varying the endpoint of the etching process [55,57].

Using hexagonal polystyrene monolayers as lithographic masks Boneberg et al. [202] found out two other types of structures, in addition to the aforementioned triangular posts. These are hillocks (nano-dots) representing residual material from detached latex particles, and nano-rings found around the original location of the polystyrene spheres on the substrate. The hillocks appear as a consequence of the strong adhesion of the spheres to the surface, while the rings originate from organic solutes in the aqueous suspension, which are deposited after the evaporation of water. It was suggested to use these structures as fluorescent dye rings of submicron size [202].

Burmeister et al. [199] investigated the possibility to induce crystal symmetries other than simply hexagonal. To achieve this a prestructured substrate could be used. By means of optical lithography silicon grids were fabricated as substrates. A periodic series of parallel trenches were created on the silicon surface; depending on the period of this grid, hexagonal or quadratic packing of deposited particles was obtained.

Xia et al. [200] described several methods that generate patterned relief structures for casting the elastomeric stamps needed in *microcontact printing*. The stamps, made from poly-dimethylsiloxane (PDMS), can be used in combination with selective wet etching to generate patterns in thin films of silver and gold. The schematic procedure for preparation of stamps with the help of 2D array from polystyrene spheres (diameter $\approx$ 200 nm) is shown in Fig. 13.36. First the 2D array is formed by evaporation from a latex suspension film (see Section 13.3). Then the particle array is covered with PDMS; finally, two types of stamps can be prepared (Fig. 13.36), which produce patterns complementary to each other [200].

Semiconducting materials having surface pores of size from tens to hundreds of nanometers, which are called *nanostructured* or *mesostructured materials*, have recently found various technological applications. Some examples are photo-electrochemical solar cells [203-205], high-performance photocatalytic films [206], sensors [207] and electrocatalysts [208-210].

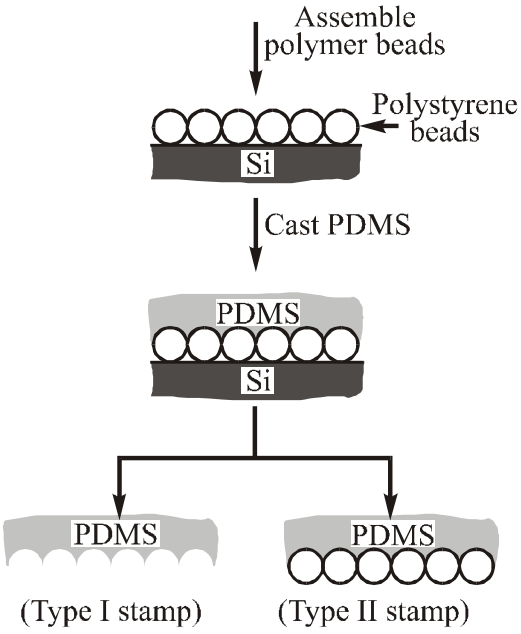

Fig. 13.36. Scheme of the procedure used by Xia et al. [200] for casting PDMS stamps from 2D array of polystyrene microspheres assembled on a planar Si substrate.

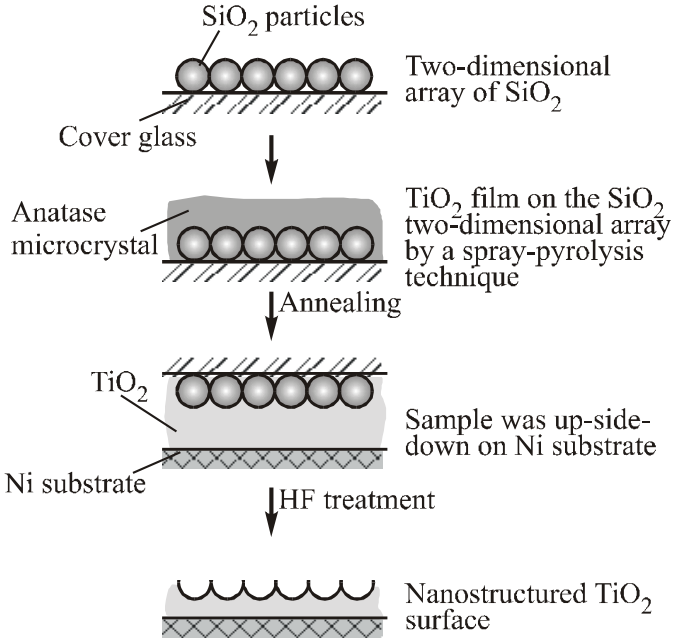

Fig. 13.37. Scheme of the procedure used by Matsushita et al. [213] for fabrication of nanostructured TiO_2 surfaces with the help of ordered 2D arrays of SiO_2 spheres.

Mesoporous TiO_2 materials, which exhibit photocatalytic properties, have been obtained by replication of 3D latex particle arrays produced via ultracentrifugation [211] or filtration [212]. Matsushita et al. [213] produced a new nanostructured TiO_2 surface by using a 2D array-based template and examined its photocatalytic activity; see also Ref. [181]. Their procedure for surface fabrication is schematically presented in Fig. 13.37. First, a 2D array from SiO_2 particles (530 nm in diameter) is created on a glass plate by means of the method of continuous deposition depicted in Fig. 13.29, Section 13.6.2. Second, the 2D array is covered with a micrometer-thick TiO_2 film, which is deposited by a spray-pyrolysis technique. Third, the TiO_2 film was fixed to a Ni substrate by epoxy for preservation of the obtained fragile structure. Next, the glass plate and the SiO_2 particles were dissolved by treatment with HF solution, which does not dissolve TiO_2 , epoxy or Ni. The photocatalytic activity of the produced mesostructured surface was tested by means of photoreduction of Ag^+ to produce silver particles [181].

13.8.3. PROTEIN 2D ARRAYS IN APPLICATIONS

As already mentioned, one of the major application of protein 2D arrays is in *electron microscope crystallography* for determining the tertiary structure of the protein molecules [146-152, 214]. A biomedical application, which may find a wide usage, is to employ 2D arrays as immunosensors and immunoassays [134-137].

Immunosensors represent a particular type of biosensor that are based on the recognition properties of antibodies (usually globular proteins). By means of the protein-engineering techniques (hybridization and cloning) it is possible to produce antibodies capable of recognizing and binding almost any type of molecule or antigen; for more details see Refs. [215, 216]. As an example, in Fig. 13.38 we present a sketch of an optical immunosensor. It can be based on the total internal reflection fluorescence (TIRF) [217, 218] or on the surface plasmon resonance (SPR) [219]. In the TIRF-based immunosensors a 2D array of antibodies is deposited on the surface of an optic fiber. After the binding of fluorescent antigens to adsorbed antibodies, one can register the fluorescence excited by the evanescent-light wave, which is located in a close vicinity of the solid substrate. The experimental studies have indicated picomolar to micromolar detection limits of this method [215, 218]. Gravimetric immunosensors, based on surface acoustic wave, have been also developed; they employ a protein 2D array adherent to the surface of a quartz piezocrystal [220].

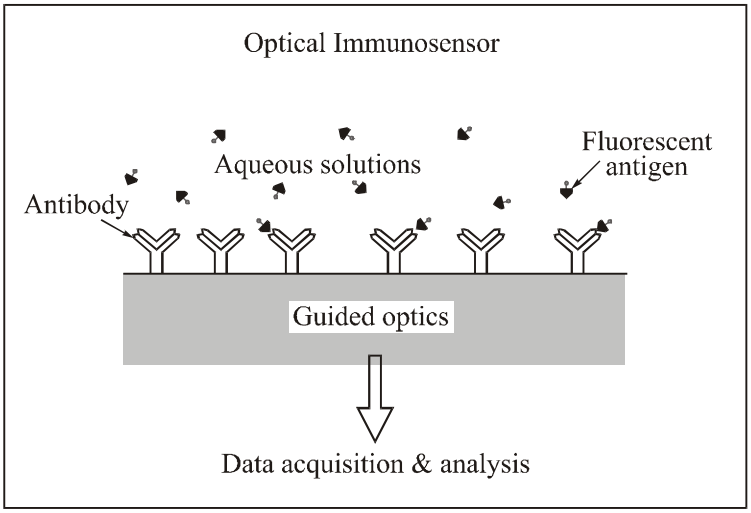

Fig. 13.38. Sketch of an optical immunosensor based on TIRF technique; after Ref. [215].

Several applications of natural ordered protein 2D arrays, present in the membranes of numerous kinds of bacteria, have been proposed. These most commonly observed bacterial cell surface structures, termed *S-layers* by Sleytr [221], are composed from a single protein species; they completely cover the bacterial cell surface and exhibit either oblique, square or hexagonal lattice symmetry. The interaction, which assembles the protein molecules into a S-layer, is due to hydrogen bonding. Consequently, a complete disintegration of S-layers into their constituent subunits can be achieved by a treatment with H-bond breaking agent, such as guanidinium hydrochloride. After removal of the disintegrating agent (e.g. by dialysis), the protein subunits are able to recrystalize into 2D arrays either in the bulk of solution or on interfaces [223].

Most of the S-layers are 5−15 nm thick and possess identical pores of size from 2 to 6 nm. This determines their potential application as isoporous ultrafiltration membranes, which exhibit very sharp molecular exclusion limits. To produce S-layer ultrafiltration membranes, the respective protein 2D arrays are deposited on the surface of commercial microfiltration membranes of pore size < 0.5 μm [222, 223]. S-layers can be applied also as supports for Langmuir-Blodgett films and covalent attachment of macromolecules, or as carriers of artificial antigens for vaccine development [222].

Finally, we arrive at the most challenging application of 2D arrays, the *molecular electronics*, which is still in its early age. During the last decades, the technology revolution in microelectronics was based on the fact that the density of device components, packed into a single integrated circuit, had grown exponentially with the passage of time. Extrapolating this tendency one could conclude that the device size would eventually reach the atomic scale. However, the experts believe that the latter is impossible to accomplish because of limitations imposed by quantum and thermal effects [224-226]. The most advanced machinery, the living organisms, operate with functional elements having molecular dimensions. Accordingly, the accessible limit of miniaturization seems to lie in the employment of structural units and principles of architecture used by the living organisms. The performance of an animal or human brain, in comparison with the most advanced silicon based computer, is a living proof that the approach of molecular electronics is justified [226].

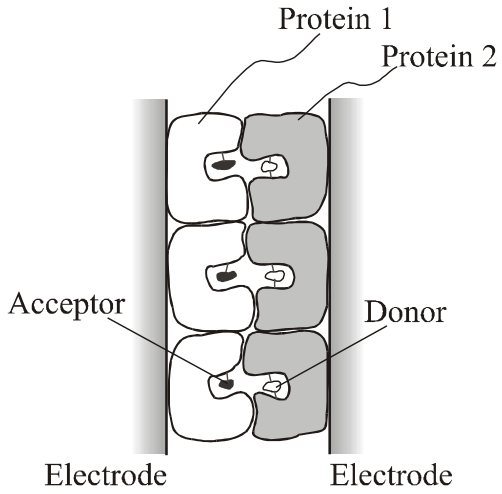

Fig. 13.39. Scheme of a protein molecular diode; after Ref. [231].

In his fine review Hong [226] notes that instead of being viewed as revolutionary technology threatening to replace conventional microelectronics, molecular electronics is to be more accurately viewed as complementary at the present stage of development. The biomaterials are mechanically delicate and chemically unstable. They easily denature and lose their functions. The living organisms operate on the principle of continuous self-repair and self-assembly, which is not attainable by the present technologies. A reasonable approach is to advance step-by-step with the development of biomolecular devices and prototypes, which at the first time may seem as clumsy hybrids between the devices of silicon-based microelectronics and the appliances of living organisms.

Proteins are the major building blocks of many functional units in the biological cells and represent important materials for building biomolecular electronic devices. For example, Aviram [227] proposed a molecular rectifier, in which different functional parts of a single protein molecule play the role of an electron donor, an insulator and an electron acceptor. A variety of designs of molecular electronic devices have subsequently appeared, exploiting either the electronic or the photonic properties of proteins [4-6, 228-231]. For example, Fig. 13.39 shows a sketch of a molecular diode (rectifier). It is composed of two protein monolayers, which possess different electronic energy levels at their electron transfer sites. Each protein monolayer is electronically linked to the surface of a supporting electrode. Thus

the electron flux between the pair of electrodes is rectified by the sandwiched protein bilayer [231].

One of the first biophotonic achievements is the development of the "Biochrom" films, which are thin-film-optical-memory devices involving the stable protein bacteriorhodopsin (bR), which is embedded into an appropriate polymeric matrix [232, 233]. These films are able to record optical information upon light exposure, to store it permanently or reversibly; they exhibit high spatial resolution, photosensitivity and cyclicity [226]. Mutated bR films have been used as holographic media [234, 235].

Miyasaka et al. [236] deposited a bR containing film on a SnO_2 conductive electrode by the Langmuir-Blodgett method. Then the bR film was put into contact with a layer of aqueous electrolyte gel and with a second gold electrode. Thus an electrochemical sandwich-type photocell was constructed, with a junction structure SnO_2/bR/electrolyte/Au. Irradiated with visible light, this photocell produced rectified photocurrent with unique differential responsivity to light intensity. Further, an artificial photoreceptor, comprising a pixel network of such bR photocells, was fabricated [236]. To ensure better orientation of the bR molecules into light-sensing photoelectric devices, antibodies were also involved in the composition of the photocells [237]. Hartley et al. [238] determined the surface potential of two-dimensional bR crystals at various pH and ionic strengths by using a silica sphere, attached to the cantilever of an atomic force microscope (AFM). A review on the photovoltaic effects in bR-containing and other biomembranes can be found in Ref. [239].

13.9. SUMMARY

The attachment of particles to an interface, accompanied with the action of lateral interparticle forces, often leads to the formation of ordered two-dimensional arrays (2D colloid crystals) from particulates or protein macromolecules. Several methods for producing such 2D arrays can be distinguished.

The most widely used approach is to evaporate the solvent from a film formed from a suspension, which contains colloidal particles or macromolecules (Section 13.1.1). The decrease of the film thickness (due to the evaporation) forces the particles to enter the liquid interface, which automatically "switches on" the powerful attraction due to the capillary

immersion force. The latter collects the particles into ordered aggregates, which further grow owing to an evaporation-driven convective influx of new particles. This method has been applied by many authors to obtain 2D crystals from proteins, viruses and various colloids.

Particle structuring is possible even in the absence of any attractive force. At sufficiently high concentration the Kirkwood-Alder phase transition occurs with both 2D and 3D systems of particles experiencing only electrostatic and/or hard-core repulsion (Section 13.1.2). Colloidal particles, which are attached to a single interface (instead of being confined into a liquid film), are not subjected to the action of the capillary immersion force, but they can also form ordered aggregates assembled by either the capillary flotation force, van der Waals attraction or Lucassen's capillary force (Section 13.1.3). Applied external electric, magnetic or optical fields can bring colloid particles to an interface and can force them to form ordered 2D arrays (Section 13.1.4). Dense monolayers of adsorbing particles acquire hexagonal packing due to the area-exclusion effect and/or attractive interparticle forces. Interfacial monolayers from insoluble molecules or particulates can be compressed to form ordered 2D arrays with the help of a Langmuir trough and can be further transferred onto a solid substrate by means of the Langmuir-Blodgett technique (Section 13.1.5).

The chapter is devoted mostly to the practical methods for preparation of particle and protein 2D arrays in evaporating liquid films. The method of the mercury trough has been applied to crystallize dozens of proteins (Section 13.2). Experiments revealing the mechanism and kinetics of 2D crystallization in evaporating films are considered in details (Section 13.3). The occurrence and advantages of 2D array formation over a liquid substrate (fluorinated oil or mercury) are described in Section 13.4. During the process of 2D crystallization a size separation of the particles occurs, which is an evidence about the action of capillary immersion forces (Section 13.5). Methods for obtaining large 2D-crystalline coatings (plate withdrawal and "brush"/extruder methods) are described in Section 13.6. Ordered particle 2D arrays can be produced also in free foam films. To observe the arrays by electron microscopy such foam films are frozen (vitrified) by a quick immersion into a cooling liquid; this electron cryo-technique ensures an excellent structure preservation of delicate vesicles or hydrated molecular complexes (Section 13.7).

The 2D arrays from colloidal particles find various applications in optics and optoelectronics (Section 13.8.1), in nano-lithography and microcontact printing, in the development of methods for fabrication of nanostructured and mesostructured surfaces for catalytic films and solar cells (Section 13.8.2). Protein 2D arrays are used for investigating molecular structure by electron microscope crystallography, for preparation of immunosensors and immunoassays, for fabrication of extremely isoporous ultrafiltration membranes, for creation of bioelectronic and biophotonic devices, etc. (Section 13.8.3).

13.10. REFERENCES

1. T. Appenzeller, Science 254 (1991) 1300.
2. G.-M. Chow, K.E. Gonsalves (Eds.) Nanotechnology: Molecularly Designed Materials, ACS, Washington, DC, 1996.
3. D. Qin, Y. Xia, J.A. Rogers, R.J. Jackman, X.-M. Zhao, G.M. Whitesides, G. M., Microfabrication, Microstructures and Microsystems, in: A. Manz and H. Becher (Eds.) Microsystem Technology in Chemistry and Life Sciences, vol. 194, Springer-Verlag, Berlin, 1998; pp. 1-20.
4. C. Nicolini, S. Carrara, P. Facci, V. Sivozhelezov, M. Adami, Molecular Bioelectronics, World Scientific, Singapore, 1996.
5. C.A. Nicolini (Ed.), Biophysics of Electron Transfer and Molecular Bioelectronics, Plenum, New York, 1998.
6. N.N. Vsevolodov, Biomolecular Electronics: An Introduction via Photosensitive Proteins, Birkhouser Publisher, Boston, 1998.
7. K. Nagayama, Adv. Biophys. 34 (1997) 3.
8. M. Ahlers, R. Blankenburg, D.W. Grainger, P. Meller, H. Ringsdorf, C. Salesse, Thin Solid Films 180 (1989) 93.
9. G.M. Whitesides, J.P. Mathias, C.T. Seto, Science 254 (1991) 1312.
10. W. Müller, H. Ringsdorf, E. Rump, G. Wildburg, X. Zhang, L. Angermaier, W. Knoll, M. Liley, J. Spinke, Science 262 (1993) 1706.
11. K. Fujita, S. Kimura, Y. Imanishi, E. Rump, J. van Esch, H. Ringsdorf, J. Am. Chem. Soc. 116 (1994) 5479.
12. D.E. Leckband, Adv. Biophys. 34 (1997) 173.
13. S. Hachisu, Y. Kobayashi, A. Kose, J. Colloid Interface Sci. 42 (1973) 342.
14. Pa. Pieranski, Phys. Rev. Lett. 45 (1980) 569.
15. I.M. Krieger, F.M. O'Neill, J. Am. Chem. Soc. 90 (1968) 3114.
16. J. Perrin, Ann. Chim. Phys. 18 (1909) 1.

17. R.C. Backus, R.C. Williams, J. Appl. Phys. 19 (1948) 1186; ibid. 20 (1949) 224; ibid. 21 (1950) 11.
18. T. Alfrey Jr., E.B. Bradford, J.W. Vanderhoff, G. Oster, J. Optical Soc. Am. 44 (1954) 603.
19. C.H. Gerould, J. Appl. Phys. 21 (1950) 183.
20. K. Nagayama, Phase Transitions 45 (1993) 185.
21. W.C. Price, R.C. Williams, R.W.G. Wyckoff, Science 102 (1945) 277.
22. V.E. Cosslett, R. Markham, Nature 161 (1948) 250.
23. R. Markham, K.M. Smith, R.W.G. Wyckoff, Nature 161 (1948) 760.
24. R.W. Horne, I. Pasquali-Ronchetti, J. Ultrastruct. Res. 47 (1974) 361.
25. R.W. Horne, Advances in Virus Research 24 (1979) 173.
26. B. Wells, R.W. Horne, P.J. Shaw, Micron 12 (1981) 37.
27. J.R. Harris, Micron 13 (1982) 169.
28. J.R. Harris, R.W. Horne, Negative staining, in: J.R. Harris (Ed.) Electron Microscopy in Biology, IRL/OUP, Oxford, 1991; p. 203.
29. J.R. Harris, Micron and Microscopica Acta 22 (1991) 341.
30. J.R. Harris, Z. Cejka, A. Wegener-Strake, W. Gebauer, J. Markl, Micron and Microscopica Acta 23 (1992) 287.
31. H. Yoshimura, S. Endo, M. Matsumoto, K. Nagayama, Y. Kagawa, J. Biochem. 106 (1989) 958.
32. H. Yoshimura, M. Matsumoto, S. Endo, K. Nagayama, Ultramicroscopy 32 (1990) 265.
33. N.D. Denkov, O.D. Velev, P.A. Kralchevsky, I.B. Ivanov, H. Yoshimura, K. Nagayama, Langmuir 8 (1992) 3183.
34. N.D. Denkov, O.D. Velev, P.A. Kralchevsky, I.B. Ivanov, H. Yoshimura, K. Nagayama, Nature (London) 361 (1993) 26.
35. C.D. Dushkin, H. Yoshimura, K. Nagayama, Chem. Phys. Lett. 204 (1993) 455.
36. C.D. Dushkin, K. Nagayama, T. Miwa, P.A. Kralchevsky, Langmuir 9 (1993) 3695.
37. G.S. Lazarov, N.D. Denkov, O.D. Velev, P.A. Kralchevsky, K. Nagayama, J. Chem. Soc. Faraday Trans. 90 (1994) 2077.
38. A.S. Dimitrov, C.D. Dushkin, H. Yoshimura, K. Nagayama, Langmuir 10 (1994) 432.
39. M. Yamaki, J. Higo, K. Nagayama, Langmuir 11 (1995) 2975.
40. A.S. Dimitrov, K. Nagayama, Langmuir 12 (1996) 1303.
41. K. Nagayama, A.S. Dimitrov, Fabrication and Application of Particle-Crystalline Films, in: T. Provder, M.A. Winnik and M.W. Urban (Eds.) Film Formation in Waterborne Coatings, ACS, Washington D.C., 1996.
42. E. Adachi, K. Nagayama, Langmuir 12 (1996) 1836.

43. S. Matsushita, T. Miwa, A. Fujishima, Langmuir 13 (1997) 2582.
44. N.D. Denkov, H. Yoshimura, K. Nagayama, Phys. Rev. Lett. 76 (1996) 2354.
45. N.D. Denkov, H. Yoshimura, K. Nagayama, Ultramicroscopy 65 (1996) 147.
46. N.D. Denkov, H. Yoshimura, T. Koyama, J. Walz, K. Nagayama, Biophys. J. 74 (1998) 1409.
47. K.P. Velikov, F. Durst, O.D. Velev, Langmuir 14 (1998) 1148.
48. H.E. Kubitschek, Nature 192 (1961) 1148.
49. U.C. Fischer, H.P. Zingsheim, J. Vac. Sci. Technol. 19 (1981) 881.
50. Y. Wang, D. Juhné, M.D. Winnik, O.M. Leung, M.C. Goh, Langmuir 8 (1992) 760.
51. R.D. Deegan, O. Bakajin, T.F. Dupont, G. Huber, S.R. Nagel, T.A. Witten, Nature 389 (1997) 827.
52. S. Maenosono, C.D. Dushkin, S. Saita, Y. Yamaguchi, Langmuir 15 (1999) 957.
53. P.C. Ohara, W.M. Gelbart, Langmuir 14 (1998) 3418.
54. J.A. Davidson, E.A. Collins, J. Colloid Interface Sci. 40 (1972) 437.
55. H.W. Deckman, J.H. Dunsmuir, Appl. Phys. Lett. 41 (1982) 377.
56. H.W. Deckman, J.H. Dunsmuir, J. Vac. Sci. Technol. B 1 (1983) 1109.
57. H.W. Deckman, J.H. Dunsmuir, S. Garoff, J.A. McHenry, D.G. Peiffer, J. Vac. Sci. Technol. B 6 (1988) 333.
58. J.C. Hulteen, R.P. van Duyne, J. Vac. Sci. Technol. A 13 (1995) 1533.
59. R. Micheletto, H. Fukuda, M. Ohtsu, Langmuir 11 (1995) 3333.
60. F. Burmeister, C. Schäfle, T. Matthes, M. Böhmisch, J. Boneberg, P. Leiderer, Langmuir 13 (1997) 2983.
61. H. Du, P. Chen, F. Liu, F.-D. Meng, T.-J. Li, X.-Y. Tang, Materials Chem. Phys. 51 (1997) 277.
62. M. Sasaki, K. Hane, J. Appl. Phys. 80 (1996) 5427.
63. L. Haggerty, B.A. Watson, M.A. Barteau, A.M. Lenhoff, J. Vac. Sci. Technol. B, 9 (1991) 1219.
64. B.A. Watson, M.A. Barteau, L. Haggerty, A.M. Lenhoff, R.S. Weber, Langmuir 8 (1992) 1145.
65. C.A. Johnson, A.M. Lenhoff, J. Colloid Interface Sci. 179 (1996) 587.
66. J.G. Kirkwood, J. Chem. Phys. 7 (1939) 919.
67. J.G. Kirkwood, E.K. Maun, B.J. Alder, J. Chem. Phys. 18 (1950) 1040.
68. B.J. Alder, T.E. Wainwright, J. Chem. Phys. 27 (1957) 1208; ibid. 31 (1959) 459; ibid. 33 (1960) 1439.
69. B.J. Alder, T.E. Wainwright, Phys. Rev. 127 (1962) 359.

70. B.J. Alder, W.G. Hoover, D.A. Young, J. Chem. Phys. 49 (1968) 3688.
71. V.G. Hoover, S.G. Gray, K.W. Johnson, J. Chem. Phys. 55 (1971) 1128.
72. M. Wadati, M. Toda, J. Phys. Soc. Japan 32 (1792) 1147.
73. S. Hachisu, Y. Kobayashi, J. Colloid Interface Sci. 46 (1974) 342.
74. A. Kose, S. Hachisu, J. Colloid Interface Sci. 46 (1974) 460.
75. J.C. Brown, P.N. Pusey, J.W. Goodwin, R.H. Ottewill, J. Phys. A, 8 (1975) 664.
76. J.C. Brown, J.W. Goodwin, R.H. Ottewill, P.N. Pusey, in M. Kerker (Ed.), Colloid Interface Science, Academic Press, New York, 1976.
77. K. Furusawa, N. Tomotsu, J. Colloid Interface Sci. 93 (1983) 504.
78. D.T. Mitchell, B.W. Ninham, B.A. Pailthorpe, J. Chem. Soc. Faraday Trans. II, 74 (1978) 1116.
79. I.K. Snook, W. van Megen, J. Chem. Phys., 72 (1980) 2907.
80. R. Kjellander, S. Marcelja, Chem. Phys Lett. 120 (1985) 393.
81. P. Tarazona, L. Vicente, Mol. Phys. 56 (1985) 557.
82. D. Henderson, J. Colloid Interface Sci. 121 (1988) 486.
83. A.D. Nikolov, D.T. Wasan, P.A. Kralchevsky, I.B. Ivanov, in N. Ise and I. Sogami (Eds.) Ordering and Organisation in Ionic Solutions, World Scientific, Singapore, 1988.
84. J.N. Israelachvili, Intermolecular and Surface Forces, Academic Press, London, 1992.
85. Pa. Pieranski, L. Strzelecki, J. Friedel, J. Phys. (Paris) 40 (1979) 853.
86. Pa. Pieranski, L. Strzelecki, B. Pansu, Phys. Rev. Lett. 50 (1983) 900.
87. B. Pansu, Pa. Pieranski, L. Strzelecki, J. Phys. (Paris) 44 (1983) 531.
88. D.H. Van Winkle, C.A. Murray, Phys. Rev. A, 34 (1986) 562.
89. C.A. Murray, D.H. Van Winkle, Phys. Rev. Lett. 58 (1987) 1200.
90. E. Kim, Y. Xia, G. M. Whitesides, J. Am. Chem. Soc. 118 (1996) 5722.
91. E. Kim, Y. Xia, G. M. Whitesides, Adv. Mater. 8 (1996) 245.
92. N. Bowden, A. Terfort, J. Carbeck, G.M. Whitesides, Science 276 (1997) 233.
93. I.E. Efremov, in E. Matijevic (Ed.) Surface and Colloid Science, Vol. 8, Wiley, New York, 1978; p. 71.
94. J. Lucassen, Colloids Surf. 65 (1992) 131.
95. B.V. Derjaguin, N.V. Churaev, V.M. Muller, Surface Forces, Plenum Press, New York, 1987.
96. A.J. Hurd, D.W. Schaefer, Phys. Rev. Lett. 54 (1985) 1043.
97. G.Y. Onoda, Phys. Rev. Lett. 55 (1985) 226.
98. M. Kondo, K. Shinozaki, L. Bergström, N. Mizutani, Langmuir 11 (1995) 394.
99. T. Heki, N. Inoue, Forma 4 (1989) 55.

100. H. Yin, H. Shibata, T. Emi, M. Suzuki, ISIJ Int. 37 (1997) 936 and 946.
101. H. Shibata, H. Yin, T Emi, Philos. Trans. Roy. Soc. London A 356 (1998) 957.
102. M. Giersig, P. Mulvaney, Langmuir 9 (1993) 3408.
103. M. Giersig, P. Mulvaney, J. Chem. Phys. 97 (1993) 6334.
104. P. Richetti, J. Prost, P. Barois, J. Phys. Lett. 45 (1984) L1137.
105. M. Trau, D.A. Saville, I.A. Askay, Science 272 (1996) 706.
106. M. Bohler, Langmuir 12 (1996) 5747.
107. S.-R. Yeh, M. Seul, B.I. Shraiman, Nature 386 (1997) 57.
108. C.D. Dushkin, T. Miwa, K. Nagayama, Chem. Phys. Lett. 285 (1998) 259.
109. P. Meakin, A.T. Skjeltop, Adv. Phys. 42 (1993) 1.
110. P. Davies, J. Popplewell, G. Martin, A. Bradbury, R.W. Chantrell, J. Phys. D: Appl. Phys. 19 (1986) 469.
111. A.S. Dimitrov, T. Takahashi, K. Furusawa, K. Nagayama, J. Phys. Chem. 100 (1996) 3163.
112. T. Takahashi, A.S. Dimitrov, K. Nagayama, J. Phys. Chem. 100 (1996) 3157.
113. M.M. Burns, J.-M. Fournier, J.A. Golovchenko, Phys. Rev. Lett. 63 (1989) 1233.
114. M.M. Burns, J.-M. Fournier, J.A. Golovchenko, Science 249 (1990) 713.
115. A. Ashkin, Science 210 (1980) 1081.
116. S. Stenholm, Rev. Mod. Phys. 58 (1986) 699.
117. J.W. Goodwin, R.H. Ottewill, A. Parentich, J. Phys. Chem. 84 (1980) 1580.
118. A.W. Adamson, A.P. Gast, Physical Chemistry of Surfaces, 6th Edition, Wiley, New York, 1997.
119. F.C. Meldrum, N.A. Kotov, J.H. Fendler, J. Phys. Chem. 98 (1994) 4506.
120. N.A. Kotov, F.C. Meldrum, C. Wu, J.H. Fendler, J. Phys. Chem. 98 (1994) 2735.
121. F.C. Meldrum, N.A. Kotov, J.H. Fendler, Langmuir 10 (1994) 2035.
122. F.C. Meldrum, N.A. Kotov, J.H. Fendler, Chem. Materials 7 (1995) 1112.
123. N.A. Kotov, G. Zavala, J.H. Fendler, J. Phys. Chem. 99 (1995) 12375.
124. C. Nicolini, V. Erokhin, F. Antolini, P. Catasti, P. Facci, Biochim. Biophys. Acta 1158 (1993) 273.
125. A. Tronin, T. Dubrovsky, C. de Nitti, A. Gussoni, V. Erokhin, C. Nicolini, Thin Solid Films 238 (1994) 127.
126. J.H. Fendler, F.C. Meldrum, Adv. Mater. 7 (1995) 607.
127. J.H. Fendler, Thin Films 20 (1995) 11.
128. P. Fromherz, Nature 231 (1971) 267.

129. L. Lebeau, E. Regnier, P. Schultz, J.C. Wang, C. Mioskowski, P. Oudet, FEBS 267 (1990) 38.

130. K. Yase, T. Udaka, Appl. Surface Sci. 60/61 (1992) 330.

131. W. Frey, W.R. Schief, D.W. Pack, C.-T. Chen, A. Chilkoti, P. Stayton, V. Vogel, F.H. Arnold, Proc. Natl. Acad. Sci. USA 93 (1996) 4937.

132. J. Miyake, M. Hara, Adv. Biophys. 34 (1997) 109.

133. O.D. Velev, Adv. Biophys. 34 (1997) 139.

134. M. Muratsugu, S. Kurosawa, N. Kamo, J. Colloid Interface Sci. 147 (1991) 378.

135. M. Muratsugu, S. Kurosawa, Y. Mori, N. Kamo, Chem. Pharm. Bull. 40 (1992) 501.

136. S. Kurosawa, N. Kamo, T. Arimura, A. Sekiya, M. Muratsugu, Mol. Cryst. Liq. Cryst. 267 (1995) 447.

137. S. Kurosawa, N. Kamo, T. Arimura, A. Sekiya, M. Muratsugu, Jpn. J. Appl. Phys. 34 (1995) 3925.

138. H. Yoshimura, T. Scheybani, W. Baumeister, K. Nagayama, Langmuir 10 (1994) 3290.

139. Z. Kam, H.B. Shore, G. Feher, J. Mol. Biol. 123 (1978) 539.

140. M. Ataka, Biopolymers 25 (1986) 337.

141. M. Ataka, M. Asai, J. Crystal Growth 90 (1988) 86.

142. T. Azuma, K. Tsukamoto, I. Sunagawa, J. Crystal Growth 98 (1989) 371.

143. V. Mikol, E. Hirsch, R. Riege, J. Mol. Biol. 213 (1990) 187.

144. M. Skouri, J.-P. Munch, B. Lorder, R. Riege, S. Candau, J. Crystal Growth 122 (1992) 14.

145. A.V. Elgersma, M. Ataka, T. Katsura, J. Crystal Growth 122 (1992) 31.

146. W. Baumeister, Ultramicroscopy 9 (1982) 151.

147. R.M. Glaeser, Ann. Rev. Phys. Chem. 36 (1985) 243.

148. R. Henderson, J.M. Baldwin, K.H. Downing, J. Lepault, F. Zemlin, Ultramicroscopy 19 (1986) 147.

149. R. Henderson, J.M. Baldwin, T.A. Ceska, F. Zemlin, E. Beckmann, K.H. Downing, J. Mol. Biol. 213 (1990) 899.

150. W. Kühlbrandt, D.H. Wang, Nature 350 (1991) 130.

151. N. Ishii, H. Yoshimura, K. Nagayama, Y. Kagawa, M. Yoshida, J. Biochem. 113 (1993) 245.

152. B.K. Jap, M. Zulauf, T. Scheybani, A. Hefti, W. Baumeister, U. Aebi, A. Engel, Ultramicroscopy 46 (1992) 45.

153. M. Yamaki, K. Matsubara, K. Nagayama, Langmuir 9 (1993) 3154.

154. K. Nagayama, Nanobiology 1 (1992) 25.

155. K. Nagayama, Colloids Surfaces A 109 (1996) 363.

156. E. Adachi, K. Nagayama, Chem. Phys. Lett. 284 (1998) 440.
157. N. Ishii, H. Taguchi, M. Yoshida, H. Yoshimura, K. Nagayama, J. Biochem. 110 (1991) 905.
158. S. Takeda, H. Yoshimura, S. Endo, T. Takahashi, K. Nagayama, Proteins 23 (1995) 548.
159. H. Yoshimura, S. Endo, K. Nagayama, M. Matsumoto, JEOL News 29E (1991) 2.
160. K. Nagayama, S. Takeda, S. Endo, H. Yoshimura, Jap. J. Appl. Phys. 34 (1995) 3947.
161. T. Scheybani, H. Yoshimura, K. Nagayama, W. Baumeister, Supramolec. Sci. 1 (1995) 111.
162. T. Akiba, H. Yoshimura, N. Namba, Science 252 (1991) 1544.
163. R. Hidalgo-Alvarez, A. Martin, A. Fernandez, D. Bastos, F. Martinez, F.J. de las Nieves, Adv. Colloid Interface Sci. 67 (1996) 1.
164. J. Conway, H. Korns, M.R. Fisch, Langmuir 13 (1997) 426.
165. J.L. Keddie, Materials Science and Engineering R, 21 (1997) 101.
166. A. van Blaaderen, P. Wiltzius, Adv. Mater. 9 (1997), 833.
167. A.H. Cardoso, C.A. Paula Leite, M.E. Darbello Zaniquelli, F. Galembeck, Colloids Surf. A 144 (1998) 207.
168. T.A. Witten, L.M. Sander, Phys. Rev. B, 27 (1983) 5686.
169. O.G. Mouritsen, Kinetics of Ordering and Growth in 2D systems, in Kinetics of Ordering and Growth at Surfaces, M.G. Lagally (Ed.), Plenum Press, New York, p.1.
170. H. Metiu, Nature 366 (1993) 111.
171. H. Röder, E. Hahn, H. Brune, J.-P. Bucher, K. Kern, Nature 366 (1993) 141.
172. E.S. Basheva, K.D. Danov, P.A. Kralchevsky, Langmuir 13 (1997) 4342.
173. J.G. Riess, M. Le Blanc, Pure Appl. Chem. 54 (1982) 2383.
174. M.-J. Stébé, G. Serratrice, J.-J. Delpuech, J. Phys. Chem. 89 (1985) 2837.
175. G. Mathis, P. Leempoel, J.-C. Ravey, C. Selve, J.-J. Delpuech, J. Am. Chem. Soc. 106 (1984) 6162.
176. M. Morita, M. Matsumoto, S. Usui, T. Abe, N.D. Denkov, O.D. Velev, I.B. Ivanov, Colloids Surf. 67 (1992) 81.
177. A.J. Durelly, V.J. Parks, Moire Analysis of Strain, Prentice-Hall, New Jersey, 1970.
178. P.C. Ohara, D.V. Leff, J.R. Heath, W.M. Gelbart, Phys. Rev. Lett. 75 (1995) 3466.
179. S. Nir, C.S. Vassilieff, in I.B. Ivanov (Ed.) Thin Liquid Films, M. Dekker, New York, 1988, p. 207.
180. S. Rakers, L.F. Chi, H. Fuchs, Langmuir 13 (1997) 7121.
181. S. Matsushita, T. Miwa, D.A. Tryk, A. Fujishima, Langmuir 14 (1998) 6441.
182. A. Scheludko, D. Exerowa, Kolloid–Z. 165 (1959) 148.

183. A. Scheludko, Adv. Colloid Interface Sci. 1 (1967) 391.
184. A.M. Poskanzer, F.C. Goodrich, J. Phys. Chem. 79 (1975) 2122.
185. L.D. Landau, E.M. Lifshitz, Statistical Physics, Part 1, Pergamon Press, Oxford, 1980.
186. P.D. Vu, J.R. Olson, R.O. Pohl, Ann. Physik 4 (1995) 9.
187. H. Ghiradella, Applied Optics 30 (1991) 3492.
188. S. Hayashi, Y. Kumamoto, T. Suzuki, T. Hirai, J. Colloid Interface Sci. 144 (1991) 538.
189. K. Nagayama, J. Phys. Soc. Japan 68 (1999) 811.
190. J. Koglin, U.C. Fischer, H. Fuchs, Phys. Rev. B 55 (1997) 7977.
191. B. Hecht, D.W. Pohl, H. Heinzemann, L. Novotny, in O. Marti and R. Möller (Eds.) Photon and Local Probes; NATO ASI Series E: Applied Sciences; Vol. 300, 1995.
192. L.T. Canham, Appl. Phys. Let. 57 (1990) 1046.
193. T. Takagahara, Surface Sci. 267 (1992) 310.
194. P.M. Bressers, J.W. Knapen, E.A. Meulenkamp, J.J. Kelley, Appl. Phys. Lett. 61 (1992) 108.
195. L.E. Brus, J. Phys. Chem. 98 (1994) 3575.
196. J.R. Heath, Science 270 (1995) 1315.
197. C.B. Murray, C.R. Kagan, M.G. Bawendi, Science 270 (1995) 1335.
198. C.R. Kagan, C.B. Murray, M. Nirmal, M.G. Bawendi, Phys. Rev. Lett. 76 (1996) 1517.
199. F. Burmeister, C. Schäfle, B. Keilhofer, C. Bechinger, J. Boneberg, P. Leiderer, Adv. Mater. 10 (1998) 495.
200. Y. Xia, J. Tien, D. Qin, G.M. Whitesides, Langmuir 12 (1996) 4033.
201. U.C. Fischer, H.P. Zingsheim, J. Vac. Sci. Technol. 19 (1981) 881.
202. J. Boneberg, F. Burmeister, C. Schäfle, P. Leiderer, D. Reim, A. Fery, S. Herminghaus, Langmuir 13 (1997) 7080.
203. A. Hagfeldt, M. Grätzel, Chem. Rev. 95 (1995) 49.
204. H. Lindstrom, H. Rensmo, S. Sodergren, A. Solbrand, S.E. Lindquist, J. Phys. Chem. 100 (1996) 3084.
205. G.K. Boschloo, A. Goossens, J. Phys. Chem. 100 (1996) 19489.
206. K.R. Gopidas, M. Bohorques, P.V. Kamat, J. Phys. Chem. 94 (1990) 6435.
207. P. Hoyer, H. Masuda, J. Mater Sci. Lett. 15 (1996) 1228.
208. P. Hoyer, Langmuir 14 (1996) 1411.
209. I. Moriguchi, H. Maeda, Y. Teraoka, S. Kagawa, Chem. Mater. 9 (1997) 1050.
210. B.B. Lakshmi, P.K. Dorhout, C.R. Martin, Chem. Mater. 9 (1997) 857.
211. J.E.G.J. Wijnhoven, W.L. Vos, Science 281 (1998) 802.
212. B.T. Holland, C.F. Blanford, A. Stein, Science 284 (1998) 538.

213. S. Matsushita, T. Miwa, A. Fujishima, Chem. Lett. 309 (1997) 925.

214. Y. Kimura, D.G. Vassylyev, A. Miyazawa, A. Kidera, M. Matsushima, K. Mitsuoka, K. Murata, T. Hirai, Y. Fujiyoshi, Nature 389 (1997) 206.

215. D. de Rossi, A. Ahluwalia, M. Mulè, IEEE Eng. Med. Biol. 13 (1994) 103.

216. M. Aizawa, Anal. Chim. Acta 250 (1991) 249.

217. J.D. Andrade, R.A. Vanwagenen, D.E. Gregoris, K. Newby, J.N. Lin, IEEE Trans. Electronic Devices 32 (1985) 1175.

218. R.M. Sutherland, C. Dahne, J.F. Place, A.R. Ringrose, J. Immunol. Meth. 74 (1984) 253.

219. J.M. Sadowsky, Proc. SPIE: Optical Testing and Metrology II, 954 (1988) 413.

220. V.V. Erokhin, R. Kayushina, Yu. Lvov, L. Feigin, Studia Biophysica 139 (1989) 120.

221. U.B. Sleytr, International Review of Cytology 53 (1978) 1.

222. P. Messner, U.B. Sleytr, Crystalline Bacterial Cell-Surface Layers, in A.H. Rose (Ed.) Advances in Microbial Physiology, Vol. 33, Academic Press, London, 1992; p.213.

223. U.B. Sleytr, D. Pum, M. Sára, Adv. Biophys. 34 (1997) 71.

224. R.W. Keyes, Physical Limits in Digital Electronics, Proc. IEEE 63 (1975) 740.

225. A. Chiabrera, E. di Zitti, F. Costa, G.M. Bisio, J. Phys. D: Appl. Phys. 22 (1989) 1571.

226. F.T. Hong, Organized Monolayer Assemblies, IEEE Eng. Med. Biol. 13 (1994) 33.

227. A. Aviram (Ed.), Molecular Electronics – Science and Technology, Engineering Foundation, New York, 1989.

228. F.T. Hong (Ed.), Molecular Electronics; Biosensors and Biocomputers, Plenum Press, New York, 1989.

229. J. Jortner (Ed.), Molecular Electronics: A "Chemistry for the 21st Century" Monograph (Iupac Chemistry for the 21st Century Series), Blackwell Sci. Inc., Boston, 1997.

230. A. Aviram (Ed.), Molecular Electronics – Science and Technology, New York Academy of Sciences, New York, 1998.

231. M. Aizawa, IEEE Eng. Med. Biol. 13 (1994) 94.

232. N.N. Vsevolodov, A.B. Druzhko, T.V. Djukova, in F.T. Hong (Ed.), Molecular Electronics; Biosensors and Biocomputers, Plenum Press, New York, 1989, p. 381.

233. N.N. Vsevolodov, A.B. Druzhko, T.V. Djukova, Proc. Ann. Int. Conf. IEEE Engng. Med. Biol. Soc. 11 (1989) 1327.

234. N. Hampp, C. Bräuchle, D. Oesterhelt, MRS Bull. 17 (1992) 56.

235. N. Hampp, D. Zeisel, IEEE Eng. Med. Biol. 13 (1994) 67.

236. T. Miyasaka, K. Koyama, I. Itoh, Science 255 (1992) 342.

237. K. Koyama, N. Yamaguchi, T. Miyasaka, Science 265 (1994) 762.

238. P. Hartley, M. Matsumoto, P. Mulvaney, Langmuir 14 (1998) 5203.

239. F.T. Hong, Photovoltaic Effect in Biomembranes, IEEE Eng. Med. Biol. 13 (1994) 75.